Real-time immune cell interactions in target tissue during autoimmune-induced damage and graft tolerance

Jason Miska,[1] Midhat H. Abdulreda,[2,3] Priyadharshini Devarajan,[1] Jen Bon Lui,[1] Jun Suzuki,[1] Antonello Pileggi,[1,2,3,4] Per-Olof Berggren,[3,5] and Zhibin Chen[1,3]

[1]Department of Microbiology and Immunology and [2]Department of Surgery, [3]Diabetes Research Institute, University of Miami Miller School of Medicine, Miami, FL 33136
[4]Department of Biomedical Engineering, University of Miami, Coral Gables, FL 33124
[5]The Rolf Luft Research Center for Diabetes and Endocrinology, Karolinska Institutet, SE-171 76 Stockholm, Sweden

Real-time imaging studies are reshaping immunological paradigms, but a visual framework is lacking for self-antigen-specific T cells at the effector phase in target tissues. To address this issue, we conducted intravital, longitudinal imaging analyses of cellular behavior in nonlymphoid target tissues to illustrate some key aspects of T cell biology. We used mouse models of T cell–mediated damage and protection of pancreatic islet grafts. Both $CD4^+$ and $CD8^+$ effector T (T_{eff}) lymphocytes directly engaged target cells. Strikingly, juxtaposed β cells lacking specific antigens were not subject to bystander destruction but grew substantially in days, likely by replication. In target tissue, $Foxp3^+$ regulatory T (T_{reg}) cells persistently contacted T_{eff} cells with or without involvement of $CD11c^+$ dendritic cells, an observation conciliating with the in vitro "trademark" of T_{reg} function, contact-dependent suppression. This study illustrates tolerance induction by contact-based immune cell interaction in target tissues and highlights potentials of tissue regeneration under antigenic incognito in inflammatory settings.

CORRESPONDENCE
Zhibin Chen:
zchen@med.miami.edu.

Abbreviations used: ACE, anterior chamber of the mouse eye; T_{eff}, effector T cells; T_{reg}, regulatory T cells.

Tissue damage by self-antigen–specific T lymphocytes causes autoimmune diseases such as type 1 diabetes. In these disorders, defective central tolerance (Mathis and Benoist, 2004) and peripheral regulation (Josefowicz et al., 2012) lead to initiation of autoantigen-specific responses in a cascade of molecular and cellular interactions between antigen-presenting cells and T lymphocytes. During the effector phase, activated $CD4^+$ and $CD8^+$ T_{eff} cells migrate to target tissues to inflict damage. The immune destruction at this phase can be suppressed by $CD4^+Foxp3^+$ T_{reg} cells (Josefowicz et al., 2012), as demonstrated in models of autoimmune diabetes (Chen et al., 2005; Feuerer et al., 2009). Extensive studies have contributed to the understanding of immune responses at the induction phase in lymphoid organs; however, the behavior of immune cells in nonlymphoid target tissues remains murky.

High-resolution imaging of live cells in lymphoid organs has elucidated key features of cellular dynamics during the initiation phase of immune responses (Germain et al., 2012). A major gap of knowledge remains, however, in understanding immune cell action and interaction in nonlymphoid target tissues, except in some infection models. In particular, noninvasive real-time evidence of how pathogenic immune cells at the effector phase engage target cells, how immune damage is controlled, and how target tissue cells respond remains scanty. This is largely a result of technical limitations that make most target tissues inaccessible to noninvasive visualization at cellular levels. Researchers often have to resort to surgical exposure of tissue or invasive insertion of a probe during imaging. Surgical wounds, however, create a two-pronged limitation on imaging analyses. First, they make

J. Miska and M.H. Abdulreda contributed equally to this paper.

J. Suzuki's present address is Dept. of Rheumatology and Internal Medicine, Juntendo University School of Medicine, Tokyo, Japan.

The Rockefeller University Press $30.00
J. Exp. Med. 2014 Vol. 211 No. 3 441-456
www.jem.org/cgi/doi/10.1084/jem.20130785

The Journal of Experimental Medicine

longitudinal analyses difficult, if possible. Second, the acute surgical wound leads to immediate release of an array of inflammatory cytokines that may confound the interpretation of immune cell behavior uncovered in a traumatic setting. As a result, key events in the cascade of $CD4^+$ and $CD8^+$ T cell–mediated immune damage or protection in target tissue remain poorly delineated.

A recently established imaging platform, intravital microscopy of pancreatic islets engrafted in the anterior chamber of the mouse eye (ACE), facilitated high-resolution visualization of immune cells noninvasively and longitudinally (Speier et al., 2008a,b; Abdulreda et al., 2011). In this study, we take advantage of this imaging platform, along with a series of reductionist animal models. We established models of effective immune responses in the ACE imaging site versus the native pancreas, in terms of equivalent kinetics of tissue damage and regulatory T (T_{reg}) cell–mediated protection. Using this noninvasive imaging approach, we studied in real time how self-antigen–specific T cells interacted with target tissue cells in vivo. We depicted the behavior of three major T cell lineages ($CD4^+$ effector T [T_{eff}] cells, $CD4^+$ T_{reg} cells, and $CD8^+$ T_{eff} cells), analyzed the regulatory effect of CTLA4 on their behavior, and examined tissue responses in destructive settings.

RESULTS

Noninvasive imaging of T cells in ACE without hindrance by the putative immunoprivilege

To study $CD4^+$ T cell responses in target tissue, we used $CD4^+$ T_{eff} and T_{reg} cells from the NOD.BDC2.5 TCR transgenic mice (Katz et al., 1993), with a specificity against a natural antigen in the pancreatic islet β cells, chromogranin A (Stadinski et al., 2010). ACE offers the technical advantage of noninvasive access and high resolution in vivo imaging, but studies using ACE could be complicated by a status of immune privilege attributed to this compartment of the eye (Benhar et al., 2012). To test whether this impacts on the immune responses of antigen-specific T cells in the islet grafts in ACE, we compared the frequency of immune damage by BDC2.5 $CD4^+$ T_{eff} cells against β cells in the ACE graft and that in the native pancreas. Donor pancreatic islets were injected into ACE through the cornea (Speier et al., 2008a,b; Abdulreda et al., 2011) at least 2 wk before T cell transfer, to ensure stable engraftment of the islets and complete healing of the minor injection wound.

Although previous studies in other settings showed that immune cells in ACE could be impacted by the eye-associated immunoprivilege (Benhar et al., 2012), in our model we found that the β cell–specific $CD4^+$ BDC2.5 T_{eff} cells destroyed the islets in the pancreas and the islet grafts in ACE at a similar tempo. Importantly, the protective T_{reg} cells acted with a similar efficacy (~50%) in controlling T_{eff} cell damage in ACE and in the endogenous pancreas (Fig. 1, A–D). Antigen-specific T_{reg} cells have been shown to be potent suppressors in several autoimmune settings, including models of type 1 diabetes (Tisch and Wang, 2008; Shevach, 2011). The main reason that only 50% of mice were protected in our experiments was likely because of the potency of the antigen-specific T_{eff} cells,

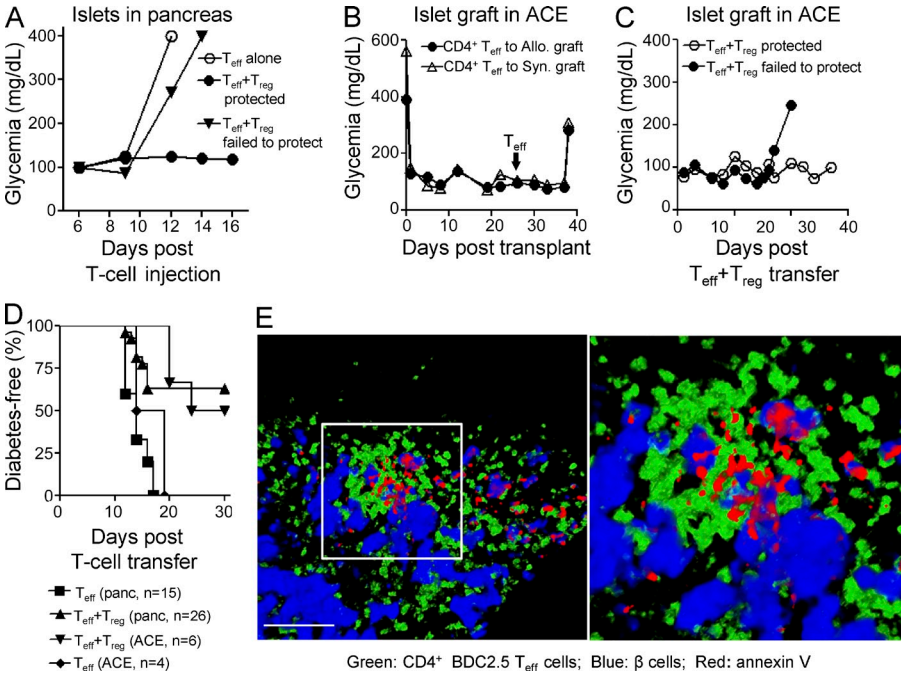

Figure 1. Noninvasive imaging in ACE was not complicated by the putative immunoprivilege and enabled visualization of the interaction between $CD4^+$ T_{eff} cells and their target cells. (A–D) The efficacies of β cell antigen–specific $CD4^+$ T_{eff} and T_{reg} cells in the endogenous pancreatic islet were compared with that of islet grafts in the anterior chamber of the eye (ACE). (A) For immune responses in native pancreata, NOD.SCID mice were injected with either BDC2.5 T_{eff} cells or T_{reg}–T_{eff} mixture. Damage to pancreatic islets was monitored by reading blood glucose (BG) levels. Animals with consecutive readings of BG > 250 mg/deciliter were considered diabetic, or failed T_{reg} cell protection if T_{reg} cells were co-transferred with T_{eff} cells. For immune responses in ACE grafts, NOD.SCID mice were rendered diabetic through streptozotocin destruction of pancreatic β cells, and then transplanted with pancreatic islets from allogeneic (B6) or syngeneic (NOD.SCID) donors into ACE. After stable engraftment (>2 wk after transplantation), $CD4^+$ T_{eff} cells alone (B) or T_{reg}–T_{eff} mixture (C) was injected into the graft-bearing mice. Graft damage was monitored by BG readings. (D) Summary of results in A–C. The cumulative incidence of diabetes was calculated for the groups of animals (n = 4–26; 2–3 experiments) presented individually in A–C. (E) 3D rendering of in vivo fluorescence micrographs for apoptotic signal Annexin V in areas of $CD4^+$ BDC2.5 T_{eff} cells engaging in direct contact with β cell targets. The results represent two experiments with a total of 4 mice analyzed with snapshot imaging of 1–3 islets per animal. Bar, 100 µm. See Video 1.

which were purified BDC2.5 $CD4^+CD25^-Foxp3^-$ cells. Nonetheless, these results are consistent with a previous study that found rejection of fully MHC-mismatched islets in ACE occurred similarly to that in a conventional extra-pancreatic implant site, the kidney sub-capsular space (Abdulreda et al., 2011). Therefore, the overall kinetics of immune destruction and protection of engrafted islet tissue in ACE was comparable to that in the native pancreas, and thus the islet grafts in ACE could serve as a surrogate in noninvasive and longitudinal imaging studies of basic T cell biology at the effector phase in the nonlymphoid target tissue.

Direct contact between antigen-specific $CD4^+$ T_{eff} cells and their target cells

$CD4^+$ T cells are categorized into several helper and regulatory subsets. Their function as killers has also been shown (Hahn et al., 1995). The in vivo capacity of $CD4^+$ T_{eff} cells killing target β cells was shown in Fig. 1 (A–D). How $CD4^+$ T cells kill remains to be fully examined. Most target tissues do not express MHC class II molecules, which are necessary for antigen-specific, cognate interaction with $CD4^+$ T cells. To study tissue destruction by antigen-specific $CD4^+$ T_{eff} cells, pancreatic islets tagged with cyan fluorescence proteins (CFP; Hara et al., 2006) were grafted in ACE. $CD4^+Foxp3^-$ BDC2.5 T_{eff} cells marked with green fluorescence proteins (GFP) were injected into the intraocular graft-bearing animals. The GFP^+CD4^+ T_{eff} cells appeared in the islet grafts and engaged in direct contact with their target β cells. We then used Annexin V in situ cytolabeling to visualize apoptosis of β cells, by injecting allophycocyanin (APC)-conjugated Annexin V into ACE. The use of this in vivo assay for β cell apoptosis was described in detail in previous works (Speier et al., 2008a,b). Apoptosis signals were present in either the contact zone between T_{eff} cells and target islet cells, or on the target islet cells with T_{eff} cells in the vicinity but not in direct contact (Fig. 1 E and Video 1). We also examined the involvement of myeloid cells at the inflammatory site, by in situ immunocytolabeling (Abdulreda et al., 2011) with anti-CD11b antibodies. We could not detect $CD11b^+$ cells in most of the areas wherein T_{eff} cells interacted with target β cells. A low frequency of $CD11b^+$ cells were found but usually in the periphery of damaged grafts. Importantly, T_{reg} cells colocalized in the protected clusters of β cells that persisted amid areas of immune damage (Fig. 2, A–C). Overall, the majority of Annexin V signals associated with β cells rather than T_{eff} cells and the amount of the apoptotic signals on β cells positively correlated with the number of T_{eff} cells at the inflammatory site (Fig. 2, D and E). The exact molecular cause of the immunopathology by the $CD4^+$ T_{eff} cells remains unclear. IFN-γ and IL-17A could be detected by flow cytometry in substantial proportions of the $CD4^+$ T_{eff} cells in the draining cervical lymph nodes of the eyes (14 ± 2 and 6 ± 1%, respectively; mean ± SEM; n = 8 mice). However, further studies are needed to determine whether these or other cytokines have a pathogenic role. The imaging data suggest that, although not exclusive, direct contact may be involved in $CD4^+$ T_{eff} cell killing of target cells, even in the absence of $CD8^+$ T_{eff} cells. The contact-dependent mode is a hallmark of cytotoxicity by $CD8^+$ T_{eff} cells.

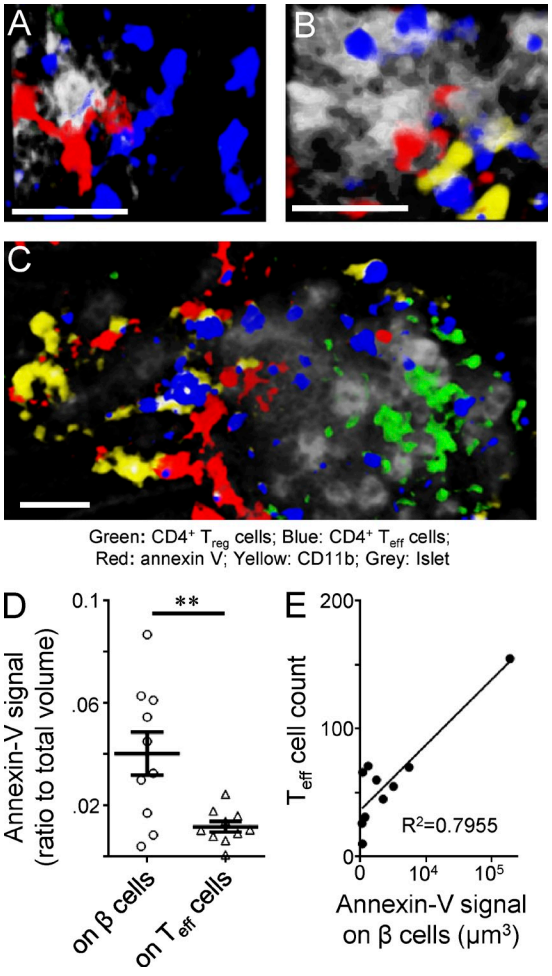

Figure 2. Direct contact between $CD4^+$ T_{eff} cells, target tissue cells and T_{reg} cells, with or without close proximity to myeloid cells. Fluorescence confocal micrographs (z-stacks) acquired within intraocular islet grafts in NOD.SCID recipients in vivo. The mice were reconstituted with CFP-labeled $CD4^+$ BDC2.5 T_{eff} cells (blue) and GFP-labeled T_{reg} cells (green), and later injected directly into ACE with BV605-conjugated anti-CD11b antibodies to label a broad subset of myeloid cells (yellow) and APC-conjugated Annexin V (red) to detect apoptotic cells in situ. The target β cells were visualized by laser backscatter (gray). (A and B) The Annexin V apoptotic signals were detected in areas of $CD4^+BDC2.5T_{eff}$ cells engaging target β cells, in the absence (A) or in the presence (B) of $CD11b^+$ myeloid cells. (C) T_{reg} cells colocalized in the protected cluster of β cells, which persisted amid rejected areas as long as T_{reg} cells existed. (D) The Annexin V signals on either β cells or T cells were measured as overlap between Annexin V stain volume and that of either β or T cells, normalized to total volume (β and T cells; mean ± SEM). (E) Linear regression analyses correlating β cell apoptosis (Annexin V signal) with the number of intra-graft T cells (n = 10 islet grafts in 4 mice). **, $P < 0.01$. Bars, 50 µm. See Video 1.

Direct engagement between CD8+ T_{eff} cells and target cells: bystander β cells were not subject to killing but grew at the interface of immune damage

We next studied noninvasive CD8+ T_{eff} cell activity in target tissue, by using CD8+ OT1 transgenic T cells (Hogquist et al., 1994), which are specific toward a model antigen, ovalbumin. Donor islets from both the RIP-mOVA transgenic mice (Kurts et al., 1996), which express ovalbumin in β cells, and the MIP-CFP mice, which lack ovalbumin but have CFP-labeled β cells (Hara et al., 2006), were grafted together in ACE of C57BL/6 (B6) animals. We selected transplanted animals that carried at least one pair of conjoined mOVA+CFP− and mOVA−CFP+ grafts like Siamese twins, and transferred them with antigen-activated CD8+GFP+ OT1 T_{eff} cells. This was done to examine antigen-specific killing versus bystander tissue destruction (Tite and Janeway, 1984). The CD8+ OT1 T_{eff} cells selectively destroyed β cells carrying the specific antigen (Fig. 3, A–C).

Strikingly, the bystander RIP-mOVA−CFP+ islets conjoined to damaged mOVA+CFP− islet grafts grew at the interface of immune destruction within days, rather than being subjected to killing (Fig. 3 A). Increase of the islet mass lacking the specific antigen required close juxtaposition with the site of antigen-specific immune responses. RIP-mOVA−CFP+ graft mass remained constant if it was not immediately adjacent (i.e., isolated) to a graft harboring the specific antigen (Fig. 3, A–C). Importantly, the increased mass of conjoined RIP-mOVA−CFP+ grafts was not a result of hypertrophy of the β cells, as the nuclear density of the conjoined and isolated islets was unchanged (Fig. S1). Moreover, imaging analyses showed preservation of the three-dimensional (3D) structure of these islets (Videos 2 and 3), precluding the possibility of imaging artifacts associated with islet flattening over time. Because the CFP expression in these islets is driven by the insulin promoter (Hara et al., 2006) and therefore labels differentiated β cells, this direct observation suggests that β cells can regenerate by replication at the site of immune damage, with an extraordinary potential of doubling in days.

Proliferation of bystander β cells in islet grafts under the kidney capsule

To examine β cell replication under inflammatory conditions in a site other than ACE, we performed our experiments using a conventional islet transplantation model. Recapitulating the settings in ACE using islets with or without specific antigens for CD8+ OT1 T_{eff} cells, B6 recipient mice were transplanted under the kidney capsule with islets from either wild-type B6 or RIP-mOVA+ transgenic donors, or a mixture of the two. The premixed islets from RIP-mOVA+ and wild-type B6 donors, or single group controls, were pelleted by centrifugation before transplantation under kidney capsule. The kidney subscapular space, although does not allow noninvasive longitudinal analyses of the same graft tissue at a cellular level, enabled the retrieval of a relatively large number of islet grafts for histological analyses.

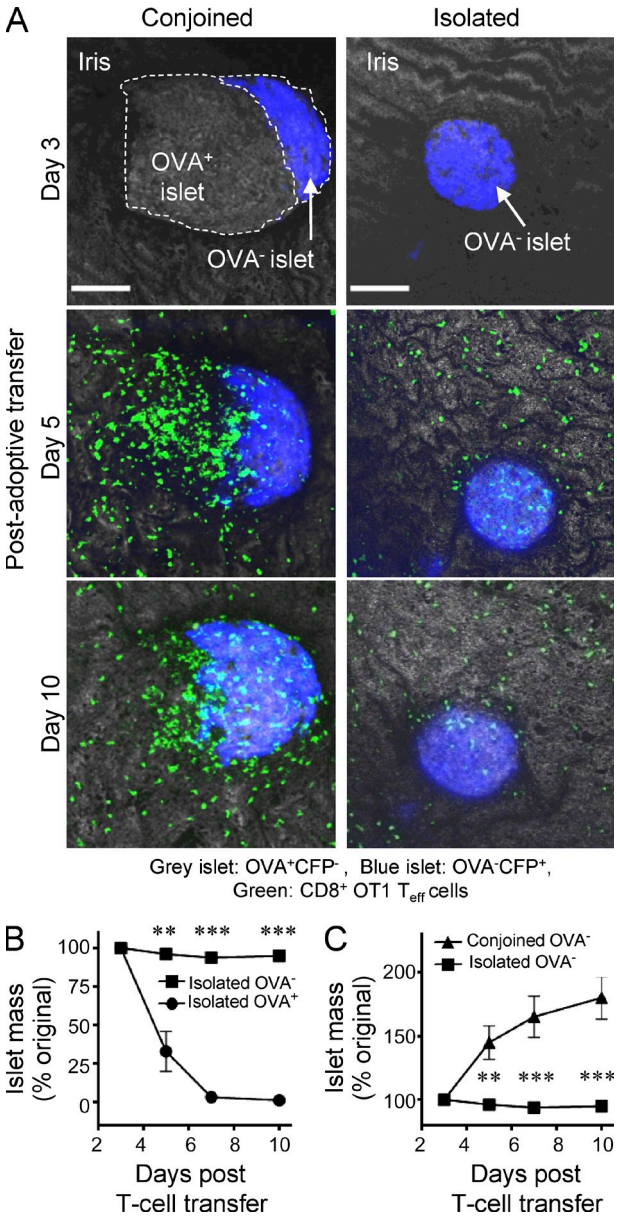

Figure 3. CD8+ T_{eff} cells damaged antigen-specific target cells but not bystander cells. (A) Longitudinal fluorescence confocal micrographs (z stacks shown as maximum projection) of islet grafts in ACE, acquired noninvasively in vivo. Visualized were infiltration and damage by OVA-specific GFP-labeled CD8+OT1 T_{eff} cells in OVA+CFP− islet grafts (gray) versus bystander OVA−CFP+ islets (blue). Data represent a total of 6 pairs of antigen-specific OVA+CFP− and nonspecific OVA−CFP+ islets conjoined like Siamese twins (left), total 6 separated OVA−CFP+ islets (right) in the same ACE environment but not conjoined with OVA+CFP− grafts, and total 6 separated OVA+CFP− islet grafts, from 5 different mice in three experiments. (B) Changes in relative islet mass (volume; mean ± SEM) of OT1 antigen-specific islets (OVA+) compared with bystander CFP islets in nonadjacent positions, after CD8+ OT1 T_{eff} cells transfer. (C) Changes in relative mass (volume; mean ± SEM) of bystander islet grafts conjoined with the specific islet graft or separated from the specific islet graft in the same ACE. Bars, 100 µm. **, $P < 0.01$; ***, $P < 0.001$. See Videos 2 and 3 for 3D islet mass visualization before and after CD8+ T_{eff} cell–mediated damage to the specific OVA+ tissue.

After engraftment of islets transplanted under the kidney capsule, the recipient animals were injected with activated $CD8^+$ OT1 T_{eff} cells, as in the animals bearing ACE grafts (Fig. 3). We then administered BrdU to the animals to label proliferating cells. The $CD8^+$ T_{eff} cells destroyed the RIP-mOVA$^+$ islet grafts. This was confirmed by microscopic examination and insulin-staining of kidney tissue sections at the site of the islet engraftment in animals transplanted with RIP-mOVA$^+$ islet alone (unpublished data). Using tissue sections of the islet grafts from the mice receiving B6 islets alone or a mixture of B6 and RIP-mOVA$^+$ islets, we conducted immunofluorescence staining to detect BrdU incorporation in the nuclei of proliferating β cells. We found that in the group with the mixed engraftment (RIP-mOVA$^+$ and B6 islets) and subsequent destruction of RIP-mOVA$^+$ islets by OT1 $CD8^+$ T_{eff} cells, there was a substantial increase in the proportion of $BrdU^+$ β cells in the remaining B6 islets, compared with the group that was transplanted with B6 islets alone (Fig. 4).

Although it cannot be determined with absolute certainty in the histological analyses whether one particular B6 islet was once in direct contact with one particular RIP-mOVA$^+$ islet after the latter was destroyed, the islets from RIP-mOVA$^+$ and wild-type B6 donors were premixed and pelleted before being implanted in the renal subcapsular space. In addition, we counted 34–36 islets in each group. Thus, increased BrdU staining in the B6 islets in the mixed transplant group, compared with that in the B6 islets alone transplant group, represents at a group level the effect of close physical proximity of the bystander B6 islets with the RIP-mOVA$^+$ islets before the latter was destroyed by OT1 T_{eff} cells. These results, obtained with a platform distinct from the ACE model, corroborated the notion that β cells lacking specific antigens are not subject to bystander killing or damage but replicate in an inflammatory setting, which is consistent with the observations from the imaging analyses of islet grafts in ACE.

T_{reg} cells interacted with T_{eff} cells through direct cell–cell contact in nonlymphoid target tissue

Immune effector function at the target tissue is controlled by various mechanisms coordinated by T_{reg} cells (Josefowicz et al., 2012). How exactly T_{reg} cells suppress immune response in vivo is still debated. Initial studies with in vitro transwell culture systems showed that T_{reg} cell suppression was effective only if T_{reg} cells were placed in the same culture chamber with T_{eff} cells and antigen-presenting cells (Takahashi et al., 1998; Thornton and Shevach, 1998). Although subsequent studies showed that T_{reg} cells could inhibit T_{eff} cell activation by modulating antigen-presenting cells (Tadokoro et al., 2006; Onishi et al., 2008; Wing et al., 2008), several in vitro studies also demonstrated that both human and murine T_{reg} cells could directly suppress T_{eff} cells independent of antigen-presenting cells (Ermann et al., 2001; Nakamura et al., 2001; Piccirillo and Shevach, 2001; Baecher-Allan et al., 2006; Hagness et al., 2012; Huang et al., 2012). However, ex vivo and in vivo imaging studies in lymph nodes did not detect stable contact between T_{reg} and T_{eff} cells (Mempel et al., 2006; Tang et al., 2006). This contradiction between in vitro and in vivo studies has left a doubt about the in vivo relevance of contact-dependent T_{reg} suppression. The in vitro trademark activity of T_{reg} cells remains to be reconciled in vivo.

In this study, we examined the pathophysiological relevance of T_{reg}–T_{eff} contact at the effector phase in the target tissue in vivo. We used the NOD.SCID reconstitution model with antigen-specific T_{reg} and T_{eff} cells that are genetically tagged with different fluorescence markers for stable labeling and longitudinal study. Adoptive transfer of T cells to lymphopenic

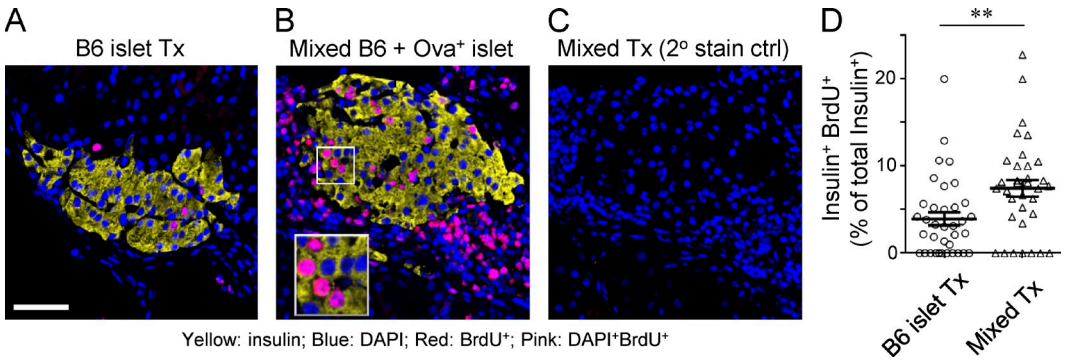

Figure 4. Analyses of islet β cell proliferation by BrdU incorporation. B6 islets, RIP-mOVA$^+$ islets, or a mixture of B6 and RIP-mOVA$^+$ islets were transplanted under the kidney capsules of B6 mice. At 7 wk after transplantation, 2×10^6 activated OT1 cells were injected i.v. into the mice. BrdU was administered by i.p injection beginning on day 2 after OT1 T cell transfer. The animals were sacrificed on day 10, and kidney tissue sections were prepared to analyze islet grafts. Tissue sections of islet grafts and surrounding kidney tissues were analyzed by immunostaining with anti-insulin and anti-BrdU antibodies and counterstained for nuclei with DAPI. The RIP-mOVA$^+$ islet graft group had a complete destruction of islet grafts, and thus it is not presented. Tissue sections of the B6 islet alone group (A) or B6 and RIP-mOVA$^+$ islets mixed engraftment group (B) were compared for insulin$^+$ cells with BrdU signals. A serial section of the latter group was also used to show the secondary staining only (C). Inset in B is the zoomed-in image of the highlighted area. The $BrdU^+$ $Insulin^-$ cells were likely the infiltrating lymphocytes that destroyed the RIP-mOVA$^+$ islets in the mixed engraftment group. (D) Data were pooled from 2 experiments with 4 mice, with 36 and 34 islets analyzed in the B6 islet alone engraftment and the mixed engraftment groups, respectively. Each data point represents one islet graft (mean ± SEM). **, $P < 0.01$. Bar, 50 µm.

animals is followed by homeostatic proliferation and activation of the transferred T cells to fill empty niches in the lymphoid organs (Surh and Sprent, 2008), which could complicate studies of T cell activation and differentiation. However, lymphopenia-associated activation is likely to have minimal impact on our study, as we focused on T cell biology at the final effector phase in the nonlymphoid target tissue, i.e., during the effector phase after activation and differentiation. The lymphopenic reconstitution model is also necessary to avoid undercounting invisible interactions (see Materials and methods) and to generate meaningful measurement of the interactive behavior among T cell subsets.

Indeed, in the T_{reg} cell–protected grafts, a majority of T_{eff} cells were in direct contact with T_{reg} cells (Fig. 5 A); they displayed a dynamic and contact-featured choreography. The interaction between the T_{reg} and T_{eff} cells usually persisted for the entire length of the imaging sessions (≥30 min) and was characterized by reduced motility (Fig. 5, A–E; and Video 4). This direct contact between T_{reg} and T_{eff} cells was not due to mere crowdedness; in tissue areas that were only sparsely infiltrated, long-lasting contact between T_{reg} and T_{eff} cells was still evident (Fig. S2).

Contact interaction between T_{reg} and T_{eff} cells with or without CD11c$^+$ DCs

T_{reg} cells can dampen the expression of the co-stimulatory molecules CD80 and CD86 on the surface of DCs, and thus inhibit T cell activation (Shevach, 2008; Wing et al., 2008). Whether the function of T_{reg} cells in the target tissue depends on DCs during the effector phase remains unclear. To examine T_{reg}–T_{eff} interaction in the context of DCs in protected

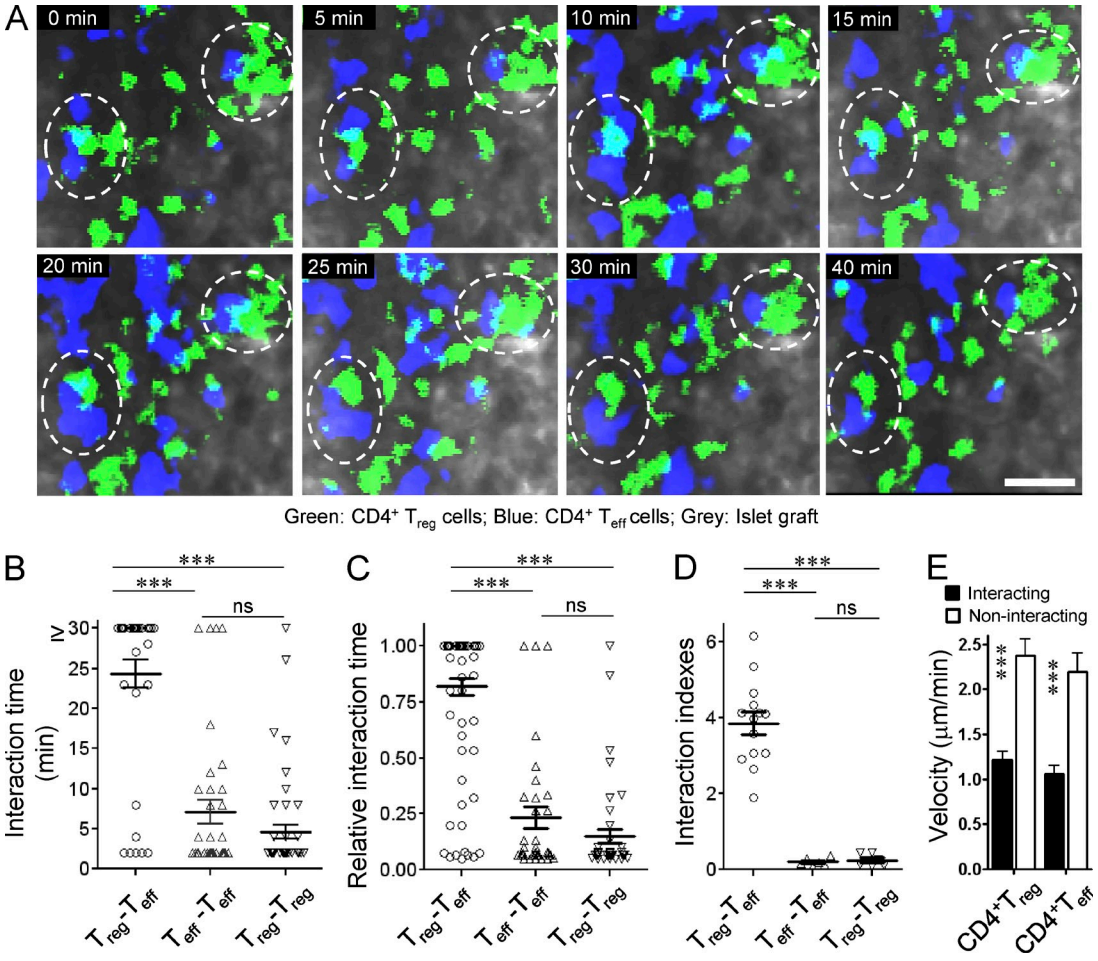

Figure 5. Noninvasive intravital visualization of T_{reg}–T_{eff} cell contact in target tissue. (A) Snapshots from representative time-lapse recordings demonstrating stable, long-lasting interaction between CD4$^+$ T_{reg}–T_{eff} interactions within the islet tissue. The majority of interactions lasted for the entire time of the recordings (≥30 min; see Video 4). Absolute (B) and relative (C) interaction time between the CD4$^+$BDC2.5 T_{eff} and T_{reg} cells (n = 50 cell pairs; mean ± SEM). Relative interaction time is calculated by dividing absolute interaction time with total imaging session length. Of note, many of the interactions were already established at the beginning of imaging; hence, actual interaction times are likely longer than those measured during the in vivo imaging timeframe which is limited by the animals' tolerance of general anesthesia. Data points represent one T_{reg}–T_{eff} pair and lines represent the mean ± SEM. The interaction index (D) and velocity (E) of both T_{eff} and T_{reg} cells in a mode of contact interaction or not (n = 55–100 cells; mean ± SEM). Data represent three experiments with 6 mice. ***, P < 0.001. Bar, 30 µm.

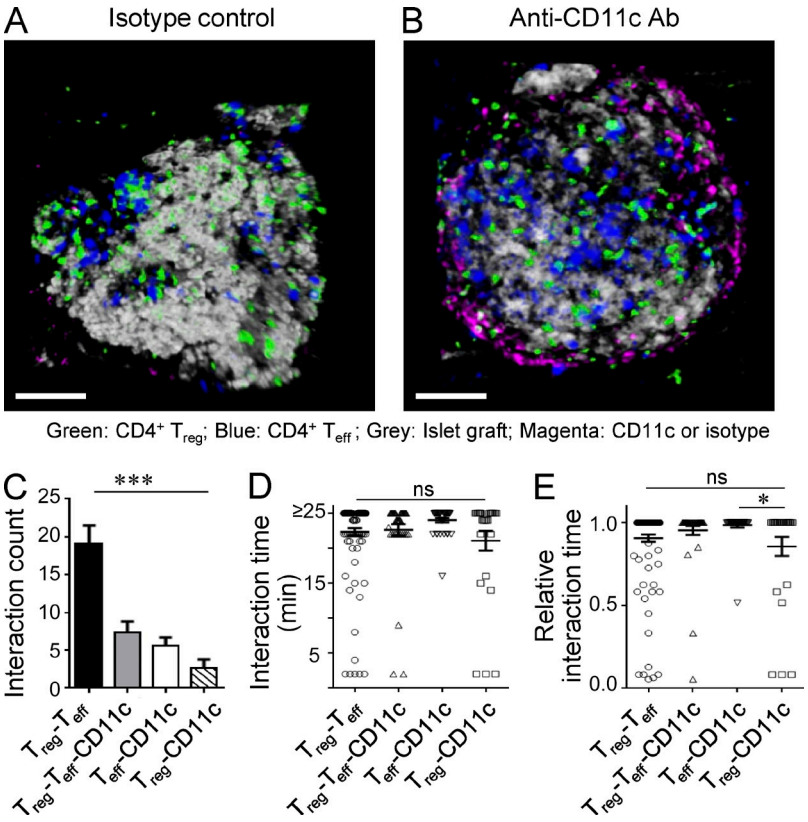

Figure 6. Stable T_{reg}–T_{eff} cell interaction with or without CD11c$^+$ DCs. (A and B) Alexa Fluor 647–labeled anti-CD11c antibodies or isotype controls were injected into ACE to visualize DCs at the site of T_{reg}–T_{eff} cell interaction in islet grafts. (C) The total count for each type of the interactions was calculated from the images in this experiment (mean ± SEM). (D) The interaction times of the different subsets in time-lapse recordings. (E) The relative interaction time is calculated by dividing absolute interaction time with total imaging session length. The data were pooled from 6 videos from three experiments with 5 mice. *, $P < 0.05$; ***, $P < 0.001$. Bar, 100 µm.

target tissues, we injected fluorescence-conjugated anti-CD11c antibodies to visualize DCs, in addition to GFP- and CFP-labeled T_{reg} and T_{eff} cells, respectively (Fig. 6, A and B). CD11c$^+$ DCs could be detected in the islet graft, mostly at the periphery (Fig. 6 B). Consequently, the majority of T_{reg}–T_{eff} cell interactions within the graft occurred in the absence of DCs, and it was also the most abundant among the various types of interactions of T_{reg}, T_{eff}, and/or CD11c$^+$ DCs. Clusters of the three types of cells, T_{reg}–T_{eff}–DC, could be detected but at a much lower frequency than that of T_{reg}–T_{eff} cell interaction without DCs. T_{eff}–DC or T_{reg}–DC interactions could be found at minor frequencies (Fig. 6 C). The interactions between T_{reg}–T_{eff} cells were also stable, with or without CD11c$^+$ DCs (Fig. 6, D and E). The interactions between CD11c$^+$ cells and T_{eff} or T_{reg} cells, although occurring in only a minor proportion of the T cells, were also mainly long lasting, with T_{reg}–CD11c$^+$ cells interactions being somewhat less stable (Fig. 6, D and E). Overall, these results show that direct contact–based interactions between T_{reg} and T_{eff} cells persisted with or without CD11c$^+$ DCs, which could reflect distinct subsets of T cells or distinct stages of the T cell function in the target tissues. The functional relevance of the different types of interactions has already been documented in vitro (Takahashi et al., 1998; Thornton and Shevach, 1998; Ermann et al., 2001; Nakamura et al., 2001; Piccirillo and Shevach, 2001; Baecher-Allan et al., 2006; Tadokoro et al., 2006; Onishi et al., 2008; Wing et al., 2008; Hagness et al., 2012; Huang et al., 2012). Our noninvasive in vivo imaging studies shows that those direct interactions do exist in vivo in target tissue. Further studies are needed to determine which interactions are most relevant in what settings for which types of functions.

T_{reg} cells persistently interacted with T_{eff} cells even when outnumbered by T_{eff} cells in damaged target tissues

Next, we examined the behavior of T_{reg} cells in a setting of failed immune regulation. We found that most T_{reg} cells at the site of extensive tissue damage were still persistently interacting with T_{eff} cells, with durations (interaction time) comparable to those in the protected tissues (Fig. 7, A and B). However, T_{reg} cells were largely outnumbered by T_{eff} cells; as a result, most T_{eff} cells were without T_{reg} cell interactions (Fig. 7, C and D). Thus, regardless of success or failure in protecting the target tissue, T_{reg} cells persistently interacted with T_{eff} cells, but an imbalance in the numbers of T_{reg} versus T_{eff} cells characterized the outcome, i.e., immune damage versus protection.

The imbalance of T_{eff} versus T_{reg} cells in the target tissue developed in some animals but not others even though they were injected with the same type of T_{reg} and T_{eff} cell mixture in the same batch of experiments. We studied the kinetics of the imbalance, taking advantage of our noninvasive platform to image both T_{reg} and T_{eff} cell populations in the same islet grafts longitudinally. The grafts were analyzed at two time points: days 10–12, when all animals were free of diabetes but had an onset of infiltration of both T_{reg} and T_{eff} cells (without substantial damage of the grafts); and days 17–20 when some animals suffered from new-onset diabetes (the islet damaged

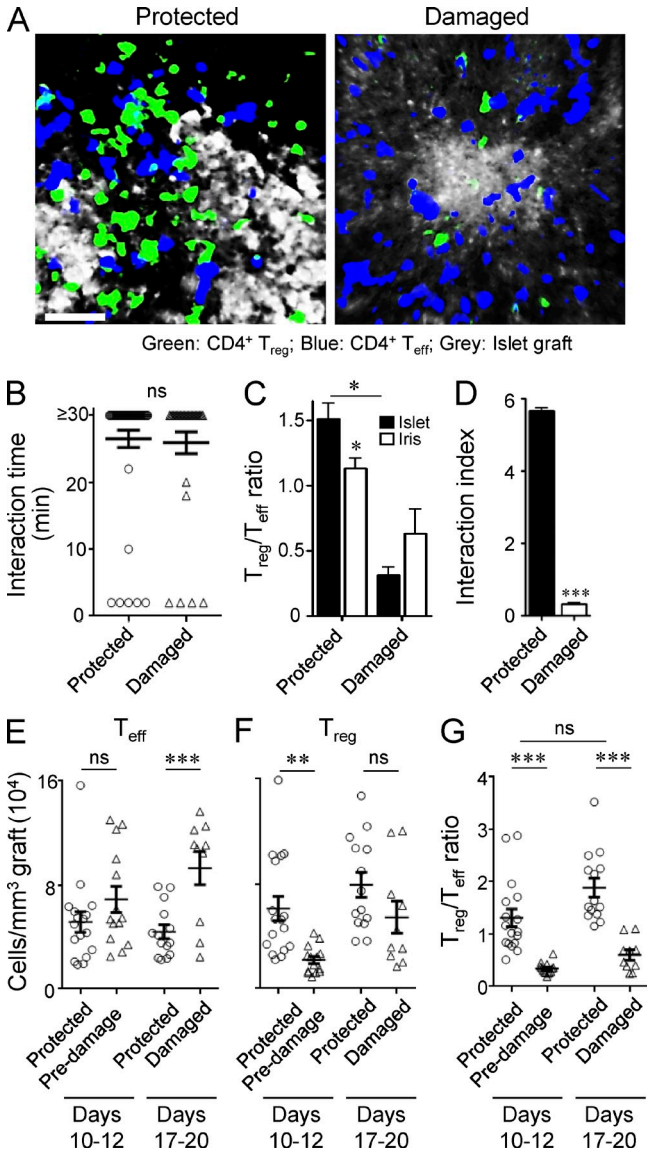

Figure 7. T_{reg} cells persistently interacted with T_{eff} cells in damaged tissue, despite an imbalance in T_{reg} versus T_{eff} numbers. $CD4^+$ T cell behavior was analyzed in the graft tissue that was being destroyed due to failed immune regulation or protected by successful T_{reg} cell regulation. Protected islet grafts had at least 80% of original islet mass, whereas damaged islet graft had 20% or less. (A) Representative fluorescence micrographs (3D rendering) showing protected (left) and damaged (right) islet grafts (gray; visualized by laser backscatter) in NOD.SCID mice reconstituted with GFP-labeled $CD4^+$ BDC2.5 T_{reg} cells and CFP-labeled $CD4^+$ BDC2.5 T_{eff} cells. (B) T_{reg}–T_{eff} interaction time in protected versus damaged grafts (mean ± SEM). (C) Ratios of T_{reg}–T_{eff} cell pairs within protected versus damaged grafts. The T_{reg}–T_{eff} cell pairs outside of the target graft tissue, in the iris in the same ACE, were analyzed as controls for the target tissue (mean ± SEM). (D) Interaction index (ratio of T_{eff} cells with or without T_{reg} interactions during the entire imaging sessions) in protected *vs.* damaged grafts (mean ± SEM). Imaging experiments in A–D were done on days 18–25 after T cell transfer. (E–G) T_{eff} and T_{reg} cell numbers in the target tissue at the initial phase of T cell infiltration (days 10–12, all animals were free of diabetes) and a later stage (days 17–20) when some animals developed diabetes with near complete (>80%) damage of the islets and some animals were protected, even though they received the same kind of T_{eff} and T_{reg} cell mixture in the same experiment. T_{eff} (E) and T_{reg} (F) cell numbers and T_{reg}/T_{eff} ratios (G) in the target tissue were analyzed in the same graft before and after extensive damage occurred (if it occurred). Results represent 3 experiments in a total of 4–6 mice in each group (the protected vs. damaged groups). Each data point represents one islet. Unpaired Student's *t* tests were performed in B and D and one-way ANOVAs with Tukey's post-hoc analyses were performed in C and E–G; *, $P < 0.05$; **, $P < 0.01$; ***, $P < 0.001$. Bar, 50 µm.

group) but other remains diabetes-free (the islet protected group). Of note, if an animal was still free of diabetes at this time point, it would remain protected for a long term, as shown in Fig. 1.

At the time point of days 10–12, the islets that would be damaged later and the islets that remain protected for a long term did not have significant difference in T_{eff} cell infiltrates (Fig. 7 E). The difference lays in the T_{reg} cells. The first group, at this predamage stage, had significantly lower numbers of T_{reg} cells compared with the protected group (Fig. 7 F). As a result, the T_{reg}/T_{eff} cell ratio was significantly reduced at this predamage time point in the would-be damaged group versus the would-be protected group (Fig. 7 G). It was only at the time point of day 17–20, when the damaged group had extensive destruction of the tissue, that the grafts had significantly more T_{eff} cells than the protected group (Fig. 7, E and G). Overall, these data show that the grafts with successful or failed T_{reg} cell protection did not have significant difference in the number of T_{eff} cells at the onset of T cell infiltration in the target tissue. These results suggest that in this experimental setting, the two different immune outcomes (graft protection or damage) are probably not caused by a difference in the numbers of T_{eff} cells expanded during the priming phase. Alternatively, the results highlighted the critical requirement of sufficient recruitment of T_{reg} cells to the inflammatory site and the continuous presence of T_{reg} cells for optimal suppression, as suggested in previous studies with models of autoimmune oophoritis (Samy et al., 2005), islet transplantation (Zhang et al., 2009), and other models of immune-mediated (Tisch and Wang, 2008; Shevach, 2011).

To further examine the behavior of T_{reg} cells in a setting of severe imbalance with T_{eff} cells, we examined the impact of acute removal of T_{reg} cells after establishment of target tissue protection. This approach also tested whether persistent contact with T_{reg} cells might impinge a lasting change of migratory behavior of T_{eff} cells. We used a $Foxp3^{DTR}$ transgenic model, which carries a diphtheria toxin (DT) receptor transgene under the control of Foxp3 promoter, enabling acute depletion of 80–90% of T_{reg} cells with a low dose of DT (Feuerer et al., 2009). In ACE islet grafts, the T_{eff} cell–mediated islet damage was suppressed by using either $Foxp3^{DTR+}$ T_{reg} cells or $Foxp3^{DTR-}$ T_{reg} controls. After stable protection of the islet grafts by the T_{reg} cells was established, the animals were treated with DT. This treatment led to an acute removal of the T_{reg} cells and a precipitous reduction in the T_{reg}/T_{eff} cell

ratio in the tissue (Fig. 8 A). The efficacy of GFP$^+$ cell removal in the islet graft indicated that the adoptively transferred GFP$^+$ cells maintained Foxp3 expression even at the effector phase in the target tissues. Depletion of T_{reg} cells led to extensive tissue damage (Fig. 8 B), and increased motility of T_{eff} cells (Fig. 8, C–E). While the residual T_{reg} cells remained in stable contact with T_{eff} cells, the T_{reg}/T_{eff} cell disproportion caused by the T_{reg}-cell depletion treatment resulted in most of the T_{eff} cells in the target tissue no longer having T_{reg}-cell partners. Thus, intimate T_{reg}–T_{eff} interaction did not irreversibly alter the aggressiveness of the T_{eff} cells.

A role of CTLA4 in T_{reg}–T_{eff} cell interaction, likely through motility regulation

The function of T_{reg} cells depends on CTLA4 (Wing et al., 2008), which also regulates T_{eff} cell function (Teft et al., 2006). We tested here the role of CTLA4 in maintaining T_{reg}–T_{eff} cell interaction by administering anti-CTLA4-antibody blockade after stable T_{reg}–T_{eff} cell interactions and T_{reg}-cell protection were established. The anti-CTLA4 treatment under this condition did not cause diabetes (data not shown). It increased T_{eff} cell numbers in the target tissue, more so than in T_{reg} cell numbers (Fig. 9, A and B), and resulted in decreased T_{reg}/T_{eff} ratios (Fig. 9, C). The treatment did not immediately disrupt the interaction between the CD4$^+$ T_{reg}–T_{eff} pairs. However, the proportion of interacting T_{reg}–T_{eff} pairs declined over time after CTLA4 blockade (Fig. 9, D), and their interaction time was shortened (Fig. 9, E and F). Although CTLA4 blockade led to increased motility of CD4$^+$ BDC2.5 T_{eff} and T_{reg} cells in T_{reg} cell–protected grafts, it decreased the motility of CD8$^+$ OT1 T_{eff} cells. Moreover, in a model wherein CTLA4 in CD8$^+$ OT1 T_{eff} cells were modulated with RNAi (Chen et al., 2006; Miska et al., 2012), CTLA4 reduction decreased motility of T_{eff} cells, suggesting an intrinsic effect of CTLA4 in T_{eff} cell motility (Fig. 10 and Videos 5 and 6). Collectively, these results suggest that CTLA4 might influence T_{reg}–T_{eff} interaction through motility regulation, but the exact effect depends on the nature of the immune settings and cell types.

DISCUSSION

Control of immune damage at the effector phase is a crucial and perhaps the most realistic therapeutic target in clinical intervention of immune-mediated diseases (Chatenoud, 2011). Improvement of therapeutic interventions will require in-depth understanding of the immune cell behavior in target tissues and of the reaction of target tissue cells in response to insult. The current study suggests that the contact-dependent mode of immune cell interaction in the target tissue is a critical part of pathophysiology at the effector phase of immune responses, and immune tolerance induction may be facilitated by promoting intimacy between pathogenic and protective immune cells. In this regard, it is highly relevant that tissue

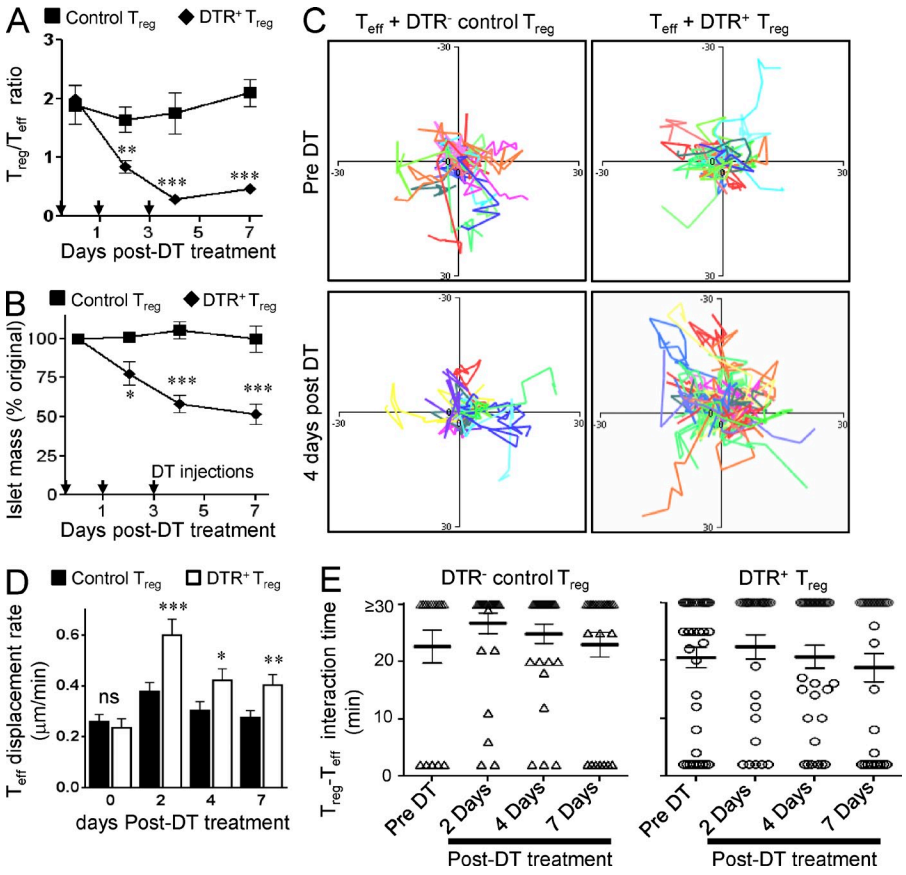

Figure 8. Acute removal of T_{reg} cells after T_{reg}–T_{eff} interaction establishment altered T_{eff} cell motility but residual T_{reg} cells maintained contact with T_{eff} cells. NOD.SCID mice with islet grafts established at the ACE site were injected with CD4$^+$ BDC2.5 T_{eff} cells, together with CD4$^+$ BDC2.5 T_{reg} cells (blue) with or without the diphtheria toxin receptor (green) at a ratio of 1:1. After establishment of protection, all mice were injected with diphtheria toxin (50 ng/g body tissue). (A and B) The effect of acute T_{reg} cell depletion (with an efficacy of ~80–90%) on T_{reg}/T_{eff} ratio (A) and tissue damage (B) after acute T_{reg} depletion (mean ± SEM). (C) The effect of T_{reg} cell removal on T_{eff} cell motility (physical displacement, flower plot of individual cell tracks), to test if T_{eff} cells exhibit altered motility after disengagement from T_{reg} cells. (D) T_{eff} cell displacement rate (μm/min; mean ± SEM). (E) The average T_{reg}–T_{eff} interaction time after acute removal of the majority of the T_{reg} cells by diphtheria toxin treatment (mean ± SEM). Data represent four mice per group from two experiments. It should be noted that the intravital imaging platform enabled us to perform noninvasive imaging at the same tissue spot in the same animal longitudinally, so the pretreatment measurements (day 0) also serve as internal controls for posttreatment measurements within each group. *, $P < 0.05$; **, $P < 0.01$; ***, $P < 0.001$.

antigen-specificity, as opposed to bystander killing (Tite and Janeway, 1984), shapes tissue fate in the effector phase.

With the tools currently available for longitudinal imaging of antigen-specific T cells in target tissues, we uncovered some basic behaviors of different lineages of T cells during the effector phase. CD8+ T cells are well known for contact-dependent killing. CD4+ T cells, on the other hand, are better known as various helper subsets, although increasing attention has been put on their potential cytotoxicity function. Although our current models do not allow us to compare the biology of CD4+ and CD8+ T cells in an ideally analogous setting, our studies provide in vivo evidence for contact-based killing of target cells by both. The observation adds to efforts to understand the behaviors of these two distinct lineages of T cells at various stages of their activation, differentiation and functioning (Mandl et al., 2012). Our results, however, do not exclude indirect mechanisms of target killing by CD4+ T_{eff} cells, and development of new tools should enable further studies to investigate such mechanisms in vivo.

It is important to make the distinction between our findings of stable T_{reg}–T_{eff} contact interaction in target tissue and those in previous reports on lack of direct T_{reg}–T_{eff} contact in lymph nodes (Mempel et al., 2006; Tang et al., 2006). T_{reg} cells play a major role in peripheral immune tolerance, likely through a variety of mechanisms (Tisch and Wang, 2008; Shevach, 2011; Josefowicz et al., 2012). However, key features of T_{reg} cell biology in vivo remain to be clarified, including whether T_{reg} cells interact with T_{eff} cells through direct contact. Two groups independently reported that T_{reg} cells could not suppress in vitro proliferation responses of T_{eff} cells if they were placed in a different chamber in a trans-well culture system (Takahashi et al., 1998; Thornton and Shevach, 1998). Although this could be attributed to an effect of T_{reg} cells on antigen-presenting cells (Tadokoro et al., 2006; Onishi et al., 2008; Wing et al., 2008), robust evidence has also been presented

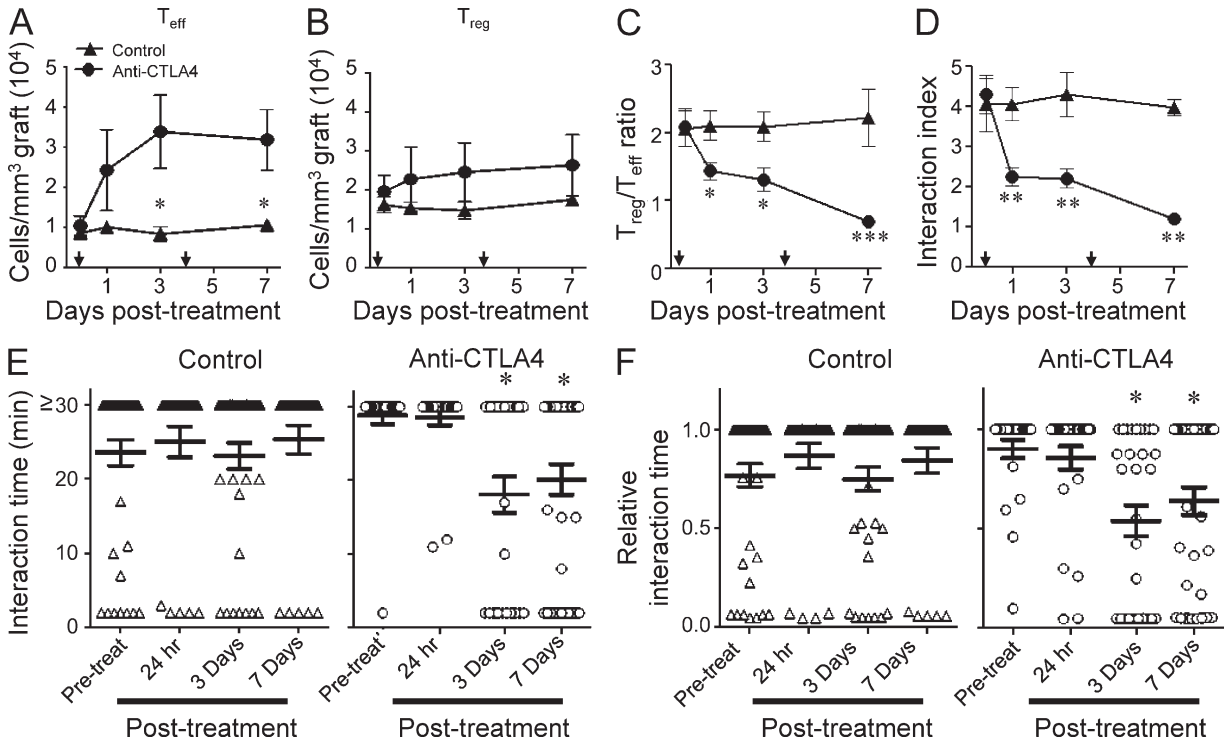

Figure 9. The effect of CTLA4 modulation on T_{reg}–T_{eff} cell interaction. NOD.SCID mice carrying islet grafts in ACE were injected with CD4+ BDC2.5 T_{eff} and T_{reg} cell mixture. After T_{reg} cell protection in the tissue was established (~30 d after T cell transfer), mice were treated with either PBS control or anti-CTLA4 monoclonal antibody (20 µg/g body weight, $n = 3$ different mice in each group). Notably, the intravital imaging platform enabled us to noninvasively image the same tissue spot in the same animal longitudinally, as in these experiments and throughout the study. Therefore, the pretreatment measurements also serve as internal controls for posttreatment measurements. (A) T_{eff} cell numbers and (B) T_{reg} cells numbers in the target tissues (mean ± SEM). (C) Intra-islet graft T_{reg}/T_{eff} cell ratio over time after anti-CTLA4 antibody blockade ($n = 10$–11 islet grafts per group per time points; mean ± SEM). (D) Interaction index, calculated as the ratio of T_{eff} cells with or without T_{reg} cell interaction, after anti-CTLA4 or control treatment (mean ± SEM). Arrows in A–D indicated injection of anti-CTLA4 antibodies. (E and F) The duration of T_{reg}–T_{eff} cell interactions after CTLA4 blockade, in actual imaging time (E) and relative to the length of whole imaging session (F; $n = 24$–40 cell pairs; mean ± SEM). One-way ANOVA across all time points in all groups did not yield statistical significance, likely because of the large variations among individual animals and time points in each group in these longitudinal imaging experiments with live animals; however, there was significant difference among pretreatment controls and posttreatment measurements within the anti-CTLA4 treatment group. *, $P < 0.05$, one way ANOVA was performed with a Tukey's multiple comparison's post-hoc analyses, compared with both pretreatment measurement of the same animal or control-treated animals. **, $P < 0.01$; ***, $P < 0.001$.

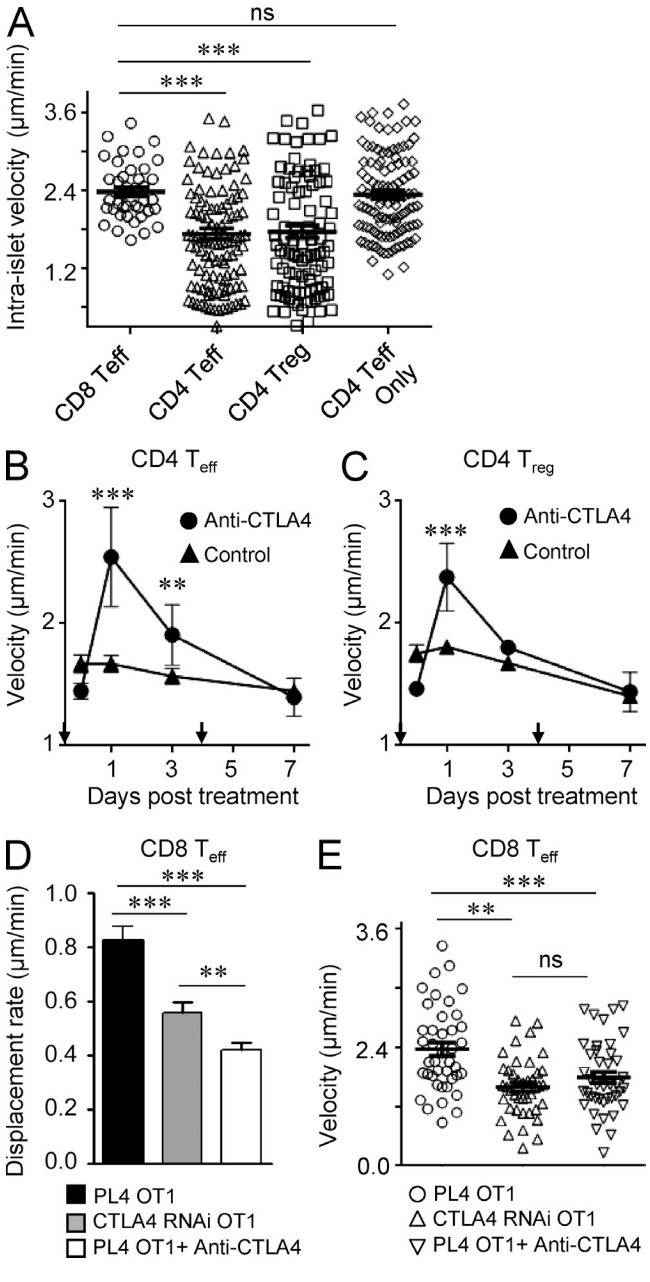

Figure 10. The effect of CTLA4 on T cell motility may depend on the type of T cells and their settings. (A) The velocity of CD8$^+$ OT1 T_{eff} cells (n = 3 mice, 40 cells, mean ± SEM) in ACE islet grafts in B6 mice is compared with that of CD4$^+$ BDC2.5 T cells in ACE islet grafts in NOD. SCID mice. For CD4$^+$ BDC2.5 T cell analyses, the CD4$^+$ T_{eff} cells (n = 5 mice, 110 cells; mean ± SEM) and CD4$^+$ BDC2.5 T_{reg} cells (n = 5 mice, 101 cells, mean ± SEM) were from animals injected either with T_{eff} and T_{reg} cell mixture (the second and third groups) or from CD4$^+$ BDC2.5 T_{eff} cells only (fourth group, n = 3 mice and 107 cells). Each dot represents one cell and the lines in plots represent mean ± SEM. (B and C) Transient change of intra-graft CD4$^+$ BDC2.5 T cell velocities after anti-CTLA4 treatment (n = 30–90 cells per group for each time point; mean ± SEM). (D and E) The effect of CTLA4 modulation on displacement (D) and velocity (E), respectively, on intra-graft CD8$^+$ OT1 T_{eff} cells. Animals were treated with anti-CTLA4 antibodies (n = 3 mice) or PBS or hamster Ig control (n = 4 mice), or they carried a CTLA4 RNAi transgene (n = 3 mice). Data represent two experiments and are from analyses of 40 cells (mean ± SEM) in each group. Each dot in E represents one cell. **, P < 0.01; ***, P < 0.001. See Videos 5 and 6.

for direct suppression T_{eff} cells by T_{reg} cells independent of antigen-presenting cells (Ermann et al., 2001; Nakamura et al., 2001; Piccirillo and Shevach, 2001; Baecher-Allan et al., 2006; Hagness et al., 2012; Huang et al., 2012), such that contact-dependent suppression has been regarded as an in vitro trademark of T_{reg} cell activity (Shevach, 2006). On the other hand, imaging analyses of explanted lymph nodes in an autoimmune diabetes animal model did not detect stable interaction between CD4$^+$ BDC2.5 T_{eff} cells and T_{reg} cells, but detected interaction between T_{reg} cell and DCs, suggesting a role of T_{reg} cells in the priming phase of T_{eff} cells (Tang et al., 2006). The suppressive effect of T_{reg} cells in the priming phase has also been documented with the findings from other studies (Tisch and Wang, 2008; Shevach, 2011). Absence of stable T_{eff}–T_{reg} cell contact in draining lymph nodes was also reported independently by another group using a different model system (Mempel et al., 2006).

In contrast, our in vivo studies focused on the effector phase in the nonlymphoid target tissue. We found that T_{reg} cells persistently interacted with T_{eff} cells through direct cell–cell contact. Importantly, the contact-based interactions between T_{reg} and T_{eff} cells in the target tissues were observed both in the presence and in the absence CD11c$^+$ DCs, although more often for the latter. In this regard, it should be noted that a previous study (Tang et al., 2006) showed that, in draining lymph nodes, although both T_{eff} cells and T_{reg} cells had stable interactions with DCs, such interactions did not lead to stable T_{reg}–T_{eff} contact. Therefore, a platform of antigen-presenting cells does not obligate direct T_{reg}–T_{eff} cell interaction. In addition, recent evidence also suggested that niche-filling homeostasis of T_{reg} cells may occur independently of DCs (Pierson et al., 2013). Nevertheless, our observations do not deemphasize the role of DCs in initiation and progression of immune damage. Homeostasis of DCs was shown to play a critical role in autoimmune damage of pancreatic islets (Dissanayake et al., 2011). In the standard NOD model of autoimmune diabetes, as well as in the BDC2.5 TCR-transgenic model, the role of DCs in initiating autoimmune diseases and their potential in tolerogenic therapies have been clearly demonstrated (Turley et al., 2003; Tarbell et al., 2007; Mukhopadhaya et al., 2008; Driver et al., 2010; Tsai et al., 2013). We believe that the visual evidence of direct T_{reg}–T_{eff} interaction in target tissue in vivo, with or without the involvement of CD11c$^+$ DCs, reconciles the discrepancy between in vitro and in vivo observations on a basic aspect of T_{reg} cell biology.

The molecular basis of T_{reg}–T_{eff} cell direct engagement remains to be elucidated. A previous study (Paust et al., 2004) reported that CD80/CD86-deficient T_{eff} cells were resistant to T_{reg} cell suppression. We explored along this line but did not detect expression of CD80 or CD86 on T_{reg} cells or T_{eff} cells in the target tissues by cytolableing in situ with specific antibodies,

nor did we find a disruptive effect on T_{reg}–T_{eff} cell interaction after injecting anti-CD80 or anti-CD86 antibodies directly into ACE (unpublished data). However, our observation in this regard is preliminary in scope and limited to the target tissue, and thus does not invalidate the hypothesis that CTLA4 expressed by T_{reg} cells may bind to CD80/CD86 on T_{eff} cells to facilitate direct cellular interactions (Paust et al., 2004). On the other hand, the data from our studies suggest that CTLA4 might affect T_{reg}–T_{eff} cell interaction through other mechanisms. A study with a conditional knockout of CTLA4 showed that T_{reg} cells require CTLA4 for functioning in vivo (Wing et al., 2008). We showed here that CTLA4 played a role in regulating T_{reg}–T_{eff} cell interaction in target tissue. This role may be related to motility regulation of both T_{reg} and T_{eff} cells. Of note, the role of CTLA4 in T cell motility control has been debated. Schneider et al. (2006) reported that CTLA4 enhanced the motility of T cells and thus reversed the stop signal originated from engaging the TCR, an effect that may preferentially impact T_{eff} cells over T_{reg} cells (Lu et al., 2012). This evidence suggested that manipulating CTLA4-based motility control could lead to therapeutic advance. Indeed, a recent study found that anti-CTLA4 antibody treatment inhibited $CD8^+$ T cell motility and promoted antitumor immunity (Ruocco et al., 2012). However, another study by Fife et al. (2009) showed that anti-CTLA4 treatment did not alter the motility of autoimmune $CD4^+$ BDC2.5 T cells in draining lymph nodes. Our imaging analyses of $CD4^+$ and $CD8^+$ T cells during the effector phase within target tissue indicate that the exact effect of CTLA4 on T cell motility may vary in different T cell subsets and may be influenced by distinct circumstance of cellular interactions.

In our experiments, CTLA4 blockade caused only modest changes on cellular interaction. It did not substantially break tolerance under the conditions we tested. The small effect on T_{reg}–T_{eff} cell interaction could be contributed by altered motility controls, although it is still a challenge to determine the cause and effect relationship in such in vivo settings. It remains to be determined how CTLA4 blockade led to an increase in T_{eff} cells, rather than T_{reg} cells, in the target tissue. The resulting imbalance of T_{reg}/T_{eff} ratios, however, did not seem likely to account for the changes in durations of T_{reg}–T_{eff} cell interactions, as reduced T_{reg}/T_{eff} ratios did not lead to reduced T_{reg}–T_{eff} interaction time in the other settings of our studies. Although these results suggest novel facets of CTLA4 function beyond the scope of this study (Han et al., 2012), they may also reconcile the debate on whether CTLA4 controls T cell motility (Schneider et al., 2006; Fife et al., 2009). Importantly, in addition to its impact on the TCR stop signals, dysregulation of CTLA4-based motility control may lead to disruption of the T_{reg}–T_{eff} cell interaction time in target tissues, which may in turn lead to exacerbated tissue damage.

Our longitudinal and noninvasive observation of live tissue in animals documented growth of healthy tissue that avoided immune cell recognition. For most target tissue cells, unlike immune cells, motility is not typically in their nature. However, they may not be mere sitting ducks in a setting of immune destruction. Rather, they may be capable of a resilient response at the inflammatory front, as illustrated by the dramatic growth of the β cells in bystander islets that were not recognized by antigen-specific T_{eff} cells. The insulin-producing β cells can regenerate through various mechanisms, which is another topic of debate. Notably, an association between microenvironment inflammation and increased β cell proliferation was recognized during insulitis and pancreatitis (Sherry et al., 2006; Cano et al., 2008; Faleo et al., 2012). A mode of β cell regeneration through replication was demonstrated in animal models, but it was evident only after months of follow up (Dor et al., 2004). A recent study (Yi et al., 2013) showed that fast replication of pancreatic β cells could be induced by treatment with an antagonist compound of insulin receptors that stimulate production of betatrophin. The intravital evidence from our study is consistent with the notion that β cells can regenerate in vivo by replication from differentiated cells, yet with a surprising rate of doubling in mass within days. The fast regeneration could be contributed to by inflammatory signals released at the interface of immune damage. Future studies are needed to uncover the molecular signals and contextual cues that led to this surprising potential of β-cell growth under antigenic incognito. These studies may ultimately aid tissue regenerative therapies in type 1 diabetes and other disorders caused by immune damage.

MATERIALS AND METHODS

Mouse models. Lines of transgenic mouse models were crossed or backcrossed to generate the necessary combinations of specific T cells and target tissue with distinct fluorescence reporters. Detailed descriptions of their genetic makeup, antigen-specificity, and fluorescence properties were provided in Table S1. NOD.BDC2.5 (Katz et al., 1993), NOD.$Foxp3^{DTR}$ (Feuerer et al., 2009), NOD.CTLA4 shRNA (CTLA4KD7; Chen et al., 2006), NOD.PL4 (Chen et al., 2006), OT1 (Hogquist et al., 1994), RIP-mOVA (Kurts et al., 1996), MIP-CFP (Hara et al., 2006) and CAG-CFP (Hadjantonakis et al., 2002) transgenic lines were described previously. The CTLA4shRNA and PL4 lines were backcrossed onto B6 background for >10 generations (Miska et al., 2012). The CTLA4shRNA transgene caused 2–3-fold reduction in CTLA4 expression. The stability of the RNAi effect in the transgenic lines on different genetic background has been established (Chen et al., 2006; Miska et al., 2012). FIR (Foxp3-IRIS-RFP knock-in) mice (Wan and Flavell, 2005) were backcrossed onto the NOD background for 10 generation to create the NOD.$Foxp3^{FIR}$ line. CAG-CFP, obtained on the C57BL/6 background, were backcrossed onto the NOD genetic background for 10 generations, and crossed with NOD.BDC2.5 and NOD.$Foxp3^{FIR}$. All animals were maintained in a specific pathogen–free barrier facility at the University of Miami, and the studies are approved by the Institutional Animal Care and Use Committee at the University of Miami.

Cell sorting and adoptive transfer. Antigen-specific $CD4^+$ BDC2.5 T_{eff} and T_{reg} cells were purified from transgenic mice on the NOD genetic background that carries the BDC2.5 transgene and the $Foxp3^{FIR}$ knock-in alleles, in combination with either the PL4 transgene for a GFP reporter or the CAG.CFP transgene for a CFP reporter. Flow cytometry staining of spleen and lymph node cells was conducted according to a standard procedure (Lu et al., 2011). T_{eff} and T_{reg} cells were sorted by using a FACSAria II flow cytometer (BD), using the following parameters: $CD4^+CD25^-$CFP (or GFP) $^+$ $BDC2.5^+CD62L^+Foxp3^{FIR-}$ for T_{eff} cells, and $CD4^+CD25^+GFP^+BDC2.5^+$ $Foxp3^{FIR+}$ for T_{reg} cells. The RFP expressed by the $Foxp3^{FIR}$ allele is used as a specific lineage marker for flow cytometry purification of T_{reg} cells, but RFP signal is not strong enough for a reliable tracking of live cells in animals.

Therefore we used an additional, nonlineage-specific GFP marker to track the cells in animals after the purified GFP$^+$Foxp3$^{R.FP+}$ cells were transferred. To enable punctuated, acute removal/depletion of Foxp3$^+$ T_{reg} cells after T_{reg}–cell protection is established, an additional transgene, Foxp3^{DTR}, the diphtheria toxin receptor (DTR) driven by a Foxp3 promoter, is crossed with NOD.BDC2.5.Foxp3^{FIR}.PL4 transgenic mice, to generate NOD.BDC2.5.Foxp3^{FIR}.PL4.Foxp3^{DTR+} mice or NOD.BDC2.5.Foxp3^{FIR}.PL4.Foxp3^{DTR-} controls. From these mice, Foxp3^{DTR+} and Foxp3^{DTR-} T_{reg} cells, respectively, were purified with CD4$^+$GFP$^+$BDC2.5$^+$Foxp3^{FIR+}CD25$^+$ markers, for adoptive transfer. Purified T_{eff} cells, or a mixture of purified T_{eff} and T_{reg} cells were injected intravenously into NOD.SCID mice, at doses of 5–10 × 10^4 cells with T_{eff}–T_{reg} ratios at 1:1. Some of the recipients had stable islet grafts established in ACE. In animals bearing islet grafts in ACE, the cervical lymph nodes draining the eyes likely play an important role in activation and differentiation of the antigen-specific T cells. The lymphopenia reconstitution model was necessary for our study, due to current limitations in tools for long-term, simultaneous tracking of different lineages of T cell in vivo. If one uses an immunocompetent animal as a recipient, rather than reconstitute a lymphopenic animal with highly purified, fluorescence-tagged T cell players, an invisible T_{reg} cell from host could be interacting with a fluorescence-tagged T_{eff} cell, but we would have to count that T_{eff} cell as if it had no T_{reg} cell interaction. That would prevent us from making meaningful conclusions on the extent of T_{reg} and T_{eff} cell interaction. Flow cytometry analyses of the recipient mice were performed to verify the stability of Foxp3 expression of the adoptive transferred T_{reg} cells ∼3 wk later, using the Foxp3-IRES-RFP reporter (Wan and Flavell, 2005).

Antigen-specific CD8$^+$ T_{eff} cells were purified from transgenic mice on the C57BL/6 background carrying the OT1 transgene and the Foxp3^{FIR} knock-in allele, in combination with the PL4 transgene for a GFP reporter, or CTLA4shRNA/PL4 transgene for a GFP reporter and CTLA4shRNA for CTLA4 RNAi knockdown. Splenocytes from the mice were stimulated with the OT1 specific ovalbumin peptide (SIINFEKL) for 24 h. CD8$^+$ T_{eff} cells were purified (>95% purity) with magnetic-bead-based cell sorting, and injected intravenously into B6 mice bearing islet grafts in ACE or under the kidney capsules.

CTLA4 blockade and acute depletion of T_{reg} cells. To examine the molecular role of CTLA4 in maintaining T_{reg}–T_{eff} cell interaction, anti-CTLA4 antibody (clone UC10-4F10-11) were injected intraperitoneally into mice, at 40 µg/g body weight, two consecutive doses at 3 d apart, after T_{reg} cell established graft protection and stable T_{reg}–T_{eff} cell interaction in the graft were detectable (typically >15 d after T cell transfer). This monoclonal antibody blocks CTLA4 function without depleting T_{reg} cells (Read et al., 2000). To test the effect of CTLA4 blockade on CD8$^+$ T_{eff} cells, one dose of anti-CTLA4 antibody was used at the time of OT1 T cell transfer into the animals. For punctual removal of diphtheria-toxin-receptor–tagged T_{reg} cells, mice carrying DTR$^+$ T_{reg} cells or control DTR$^-$ T_{reg} cells were injected (50 ng/g body weight) with DT at a schedule of day 0, 1, and 3, similar to a previously described regimen (Feuerer et al., 2009), after graft protection was established and stable T_{reg}–T_{eff} interactions were detected.

Intraocular injection of fluorescence-tagged antibodies for in situ cytolabeling. In some instances, fluorescently conjugated antibodies were injected directly into ACE for in vivo cytolabeling in situ. With our intravital imaging platform, the injected antibodies can effectively label cells up to 50 µm deep within the graft tissue, which is at the similar depth capacity for accurately tracking cells marked with genetic tags of fluorescence markers (Abdulreda et al., 2011). After mice were adoptively transferred with T_{reg} and T_{eff} cells, mice were injected with fluorochrome-conjugated antibodies directly into the anterior chamber. All antibodies were tested with isotype controls to determine specificity of the in situ labeling. The following is a list of the antibodies and their isotype controls. BV605 conjugated anti-CD11b monoclonal antibody or rat Ig2a isotype control; Alexa Fluor 647–conjugated anti-CD11c, anti-CD80, and anti-CD86 monoclonal antibodies and hamster IgG isotype control (BioLegend). APC-conjugated Annexin V (eBioscience) was used to assess apoptotic cells in ACE grafts. This in vivo assay for β cell apoptosis was described previously (Speier et al., 2008a,b).

Islet transplantation into ACE and noninvasive in vivo imaging. The pancreatic islets were transplanted into ACE by injection through the cornea, as previously described (Abdulreda et al., 2011; Speier et al., 2008a,b). The cornea serves as a natural window for noninvasive visualization of transplants. This injection procedure does not entail substantial injury to the cornea or the eye chamber. At least 2 wk were allowed for complete engraftment of the islets before any experimentation. Intravital imaging of the transplants was conducted by confocal microscopy, with a Leica upright TCS SP-5broadband confocal microscope (using Leica 20X/0.5NA HCX APO L U-V-I 12 lens for PBS immersion), as previously described (2008a,b; Abdulreda et al., 2011). T_{reg} and T_{eff} cells were visualized by GFP or CFP fluorescence. Target islet cells were visualized by laser backscatter (reflection) or CFP fluorescence 3D (xyz) or time-lapse (xyzt; 4D) noninvasive in vivo imaging was acquired longitudinally. In time-lapse recordings, z stacks were acquired every 2 min for 30–75 min and the z-spacing ranged from 5–7 µm. A key strength of this intravital imaging platform is noninvasiveness that few other intravital cellular imaging platforms have been afforded. This strength not only avoids inadvertent inflammatory signals caused by surgical exposure for imaging needs, but enables us to monitor the same tissue in the same animal longitudinally at cellular resolution. A baseline measurement serves as a rigorous, internal control for all postintervention measurements of the same live tissue in the same live animal.

Animals were routinely monitored by urine and blood glucose levels. Animals transplanted with islet grafts in ACE were examined 2 wk after transplantation for engraftment. After T cell transfer, the islet grafts in ACE were examined every 2–3 d with the imaging microscope. Animals with two consecutive readings of BG > 250 mg/deciliter were considered diabetic. With regard to individual islet grafts in ACE in setting of immune responses, a graft maintaining >80% of its original mass was considered protected, and a graft with <20% of its original mass was considered damaged or failure in immune regulation. In experiments in which a relatively small number of islets were transplanted in ACE, the islet grafts served as indicators of immune responses and the endogenous pancreatic islets maintained blood glucose homeostasis of the animals. The immune damage of islet grafts in ACE always correlated with incidence of diabetes that was caused by immune destruction of endogenous pancreatic islets.

Islet transplantation in renal subcapsular space and BrdU labeling of proliferating cells. The responses of bystander islet cells in an inflammatory setting were also examined at a transplantation site that is different from ACE, the renal subcapsular space, which is the standard transplantation site for experimental studies of islet grafts in rodent recipients. It has been an invaluable research tool for decades (Ricordi et al., 1987). It allows transplantation of islets in a well-confined location that can then be retrieved for histopathological or molecular analyses of a relatively large number of islets. Islets were transplanted under the kidney capsule of B6 mice by the Diabetes Research Institute Preclinical Cell Processing and Translational Models Core facility following standard procedures (Berney et al., 2001; Faleo et al., 2012). In brief, pancreatic islets were isolated from either wild-type B6 or RIP-mOVA$^+$ transgenic donors. B6 islets, RIP-mOVA$^+$ islets, or a mixture of B6 islets and RIP-mOVA$^+$ islets were prepared into individual aliquots for each transplant recipient. They were then handpicked with a Hamilton syringe and transferred into a polyethylene tube (PE50; BD; inside diameter 0.58 mm; outside diameter, 0.965 mm) that was kinked at one end, and then pelleted in the kinked tubing by centrifugation at 1,000 rpm for 2 min, to pack them together. The pelleting step was done before the transplantation procedure.

After induction of general anesthesia (isoflurane 2%/oxygen mix, to effect), a left flank incision was performed and the left kidney exteriorized and exposed. Under a dissection microscope and using microsurgical forceps, a small breach was performed on the capsule at the caudal pole of the kidney through which the tubing containing the pelleted islets was gently inserted and pushed toward the opposite (cranial) pole. Islets were gently released in

the renal subcapsular space under visual microscopic inspection. Next, the tubing was gently removed and the breach on the capsule cauterized to prevent back flow. The kidney was repositioned in the abdominal cavity, and the muscular and cutaneous layer sutured. The graft-bearing mice were rested for ∼7 wk after transplantation to ensure engraftment, and then adoptively transferred with activated OT1 $CD8^+$ T cells by intravenous injection. 2 d later, BrdU was injected at a concentration of 10mg/kg every 12 h. On day 10, kidneys were removed, fixed in 4% PFA overnight, followed by immersing in 30% sucrose overnight, and then embedded in OCT. Sections were cut and stained for BrdU incorporation with biotinylated antibodies against BrdU, using an in situ BrdU detection kit (BD) designed for histology use. We modified the secondary staining procedure for immunofluorescence staining. Although isotype controls were not included in the kit, we established the specificity of the BrdU staining procedure with spleen tissue sections from animals with or without BrdU injection treatment. To expose BrdU epitopes in the nuclear DNA, a covered plastic coplin (filled with 50 ml of diluted BD Retrievagen buffer) was preheated in a water bath at 95–97°C. After 30 min, the tissue slides were quickly placed into a preheated jar, and incubated for another 30 min. The tissue slides in the closed jar were then removed and left at ambient temperature for one hour. Primary anti-insulin antibodies (polyclonal guinea pig anti-insulin; DAKO; titration, 1:1,000) and the biotinylated anti-BrdU antibodies were incubated overnight with the tissue sections at 4°C, and then washed according to manufacturer's instructions. Secondary staining was done with Alexa Fluor 488–conjugated streptavidin (Life Technologies; titration, 1:500) and Alexa Fluor 647–conjugated donkey anti–guinea pig $F(ab)_2$ (Jackson ImmunoResearch Laboratories; titration, 1:500). Sections were counterstained with DAPI and mounted for fluorescence microscopy. Images were acquired with a Leica inverted TCS SP-5 broadband confocal microscope (using Leica 40×/1.25–0.75NA HCX PL APO lens for oil immersion).

Image analysis. Image analyses were performed using the Volocity software (version 6; Perkin Elmer) as previously described (Abdulreda et al., 2011). Images were denoised and contrast-enhanced equally for consistent analyses. Quantitative analyses of cellular movement and T_{reg}–T_{eff} cell interaction dynamics were performed automatically in the Volocity with user feedback on drift-corrected 3D time-lapse recordings. Drift correction was performed in Volocity based on proprietary algorithms. T cell counting and movement tracking were performed automatically by the software and dynamic parameters (e.g., velocity, displacement) were derived from time-lapse recordings. T_{reg}–T_{eff} cell interaction time and interaction index were calculated manually. The interaction time between the T_{reg}–T_{eff} cell interacting pairs was calculated manually using the time stamps embedded in each image frame in a time-lapse series. The interaction index is calculated by dividing the number of T_{eff} cells interacting with T_{reg} cells with the number of T_{eff} cells not interacting with T_{reg} cells. β cell (islet) mass was measured by the software, as previously described (Abdulreda et al., 2011), based on volume detected by either laser backscatter or CFP fluorescence.

Annexin V labeling in islet grafts in ACE was quantified with z-stack images that were acquired ∼10–15 min after injection of APC-labeled Annexin V directly into ACE. Using proprietary algorithms in Volocity, we then measured in the 3D images the amount of overlap in the volume the Annexin V–positive stain with either that of β cells (visualized by CFP or backscatter) or CFP/GFP-labeled T_{eff} cells (Rodriguez-Diaz et al., 2011). Automatic selection, optimized with user feedback, based on fluorescence of Annexin V–positive cells, β cells, and T cells and volume measurements were performed automatically by the software. The overlap (volume) in Annexin V stain with either that of β or T cells was also derived by the software, and was expressed as a fraction of the total volume of the β and T cells in each islet. Similarly, the number of graft-infiltrating T_{eff} cells was automatically measured based on fluorescence intensity (Abdulreda et al., 2011). Islet cell mass was measured using Volocity software as previously described (Abdulreda et al., 2011), based on islet volume detected either by laser backscatter (reflection) or CFP fluorescence. For example, in Fig. 3, the volume of CFP-labeled β cells was measured based on CFP fluorescence which is in this case restricted to the bystander islets in this case. In brief, a proprietary detection algorithm built into the Volocity software was used to detect CFP signal based on fluorescence intensity. The detection threshold was set with user feedback to restrict the selection to the CFP-labeled β cells. Once the selection was made, the volume was derived automatically by the software. Longitudinal analyses on the same individual islets were performed using the same approach, and numerical values of islet volumes were expressed as means ± SEM at the different time points under the different conditions.

Statistical analysis. Unpaired Student's *t* test was used to compare two samples. For multiple group comparisons, one-way ANOVA tests were performed followed up by Tukey's post-hoc multiple comparisons test. $P \leq 0.05$ was considered significant. Asterisks indicate significance (*, $P < 0.05$; **, $P < 0.01$; ***, $P < 0.001$).

Online supplemental material. Fig. S1 relates to Fig. 3 and shows digital estimation of cell nuclear density in islet grafts imaged over time in the living animal. Fig. S2 relates to Fig. 5 and shows that the long-lasting contact between T_{reg}–T_{eff} in the target tissue occurred even in areas with sparse infiltration of T cells. Table S1 lists the transgenic mouse models genetically tagged with antigen-specific T cell receptor, fluorescence reporters, and lineage markers for the imaging studies. Video 1 (corresponds to Fig. 1) shows direct interaction between antigen-specific $CD4^+$ T_{eff} cells with target β-cells in pancreatic islet grafts in ACE. Videos 2 and 3 (corresponds to Fig. 3) shows antigen-specific $CD8^+$ OT1 T_{eff} cell–mediated destruction of OVA^+ islets and concomitant growth of juxtaposed bystander OVA^- islets. Video 4 (corresponds to Fig. 5) shows stable long-lasting interaction between T_{reg} and T_{eff} cells in the target tissue. Video 5 and 6 (corresponds to Fig. 10) shows CTLA4 blockade reduces $CD8^+$ T_{eff} cell motility in target tissue. Online supplemental material is available at http://www.jem.org/cgi/content/full/jem.20130785/DC1.

This work was supported by grants from the National Institutes of Health (DP3DK085696 to Z. Chen; F32DK083226 to M.H. Abdulreda; 5U19AI050864-10 to A. Pileggi; and NIH-U-01DK089538 to A. Pileggi and P.-O. Berggren), and funds from the Diabetes Research Institute Foundation (to M.H. Abdulreda, A. Pileggi, P.-O. Berggren, and Z. Chen). Additional research support was provided through funds from the Swedish Research Council and the Family Erling-Persson Foundation (to P.-O. Berggren). The content is solely the responsibility of the authors and does not necessarily represent the official views of the funding institutions. We thank Mrs. E. Zahr-Akrawi, Mr. J. Enten, and Mr. K. Johnson, and Drs. O. Umland, G. McNamara, R.D. Molano, A. Bayer, A. Caicedo, S. Jacobs, and S. Opiela for their expert assistance and advice.

J. Miska, M.H. Abdulreda, P. Devarajan, J.B. Lui, J. Suzuki, A. Pileggi, and Z. Chen declare no financial or commercial conflicts of interest. P.-O. Berggren is one of the founders of the biotech company Biocrine, and he is also on the board of this company. Biocrine is going to use the anterior chamber of the eye as a commercial servicing platform.

Submitted: 15 April 2013
Accepted: 27 January 2014

REFERENCES

Abdulreda, M.H., G. Faleo, R.D. Molano, M. Lopez-Cabezas, J. Molina, Y. Tan, O.A. Echeverria, E. Zahr-Akrawi, R. Rodriguez-Diaz, P.K. Edlund, et al. 2011. High-resolution, noninvasive longitudinal live imaging of immune responses. *Proc. Natl. Acad. Sci. USA.* 108:12863–12868. http://dx.doi.org/10.1073/pnas.1105002108

Baecher-Allan, C., E. Wolf, and D.A. Hafler. 2006. MHC class II expression identifies functionally distinct human regulatory T cells. *J. Immunol.* 176:4622–4631.

Benhar, I., A. London, and M. Schwartz. 2012. The privileged immunity of immune privileged organs: the case of the eye. *Front Immunol.* 3:296. http://dx.doi.org/10.3389/fimmu.2012.00296

Berney, T., R.D. Molano, P. Cattan, A. Pileggi, C. Vizzardelli, R. Oliver, C. Ricordi, and L. Inverardi. 2001. Endotoxin-mediated delayed islet graft function is associated with increased intra-islet cytokine production and

islet cell apoptosis. *Transplantation*. 71:125–132. http://dx.doi.org/10.1097/00007890-200101150-00020

Cano, D.A., I.C. Rulifson, P.W. Heiser, L.B. Swigart, S. Pelengaris, M. German, G.I. Evan, J.A. Bluestone, and M. Hebrok. 2008. Regulated beta-cell regeneration in the adult mouse pancreas. *Diabetes*. 57:958–966. http://dx.doi.org/10.2337/db07-0913

Chatenoud, L. 2011. Diabetes: type 1 diabetes mellitus—a door opening to a real therapy? *Nat Rev Endocrinol*. 7:564–566. http://dx.doi.org/10.1038/nrendo.2011.148

Chen, Z., A.E. Herman, M. Matos, D. Mathis, and C. Benoist. 2005. Where CD4+CD25+ T reg cells impinge on autoimmune diabetes. *J. Exp. Med*. 202:1387–1397. http://dx.doi.org/10.1084/jem.20051409

Chen, Z., J. Stockton, D. Mathis, and C. Benoist. 2006. Modeling CTLA4-linked autoimmunity with RNA interference in mice. *Proc. Natl. Acad. Sci. USA*. 103:16400–16405. http://dx.doi.org/10.1073/pnas.0607854103

Dissanayake, D., H. Hall, N. Berg-Brown, A.R. Elford, S.R. Hamilton, K. Murakami, L.S. Deluca, J.L. Gommerman, and P.S. Ohashi. 2011. Nuclear factor-κB1 controls the functional maturation of dendritic cells and prevents the activation of autoreactive T cells. *Nat. Med*. 17:1663–1667. http://dx.doi.org/10.1038/nm.2556

Dor, Y., J. Brown, O.I. Martinez, and D.A. Melton. 2004. Adult pancreatic beta-cells are formed by self-duplication rather than stem-cell differentiation. *Nature*. 429:41–46. http://dx.doi.org/10.1038/nature02520

Driver, J.P., F. Scheuplein, Y.G. Chen, A.E. Grier, S.B. Wilson, and D.V. Serreze. 2010. Invariant natural killer T-cell control of type 1 diabetes: a dendritic cell genetic decision of a silver bullet or Russian roulette. *Diabetes*. 59:423–432. http://dx.doi.org/10.2337/db09-1116

Ermann, J., V. Szanya, G.S. Ford, V. Paragas, C.G. Fathman, and K. Lejon. 2001. CD4(+)CD25(+) T cells facilitate the induction of T cell anergy. *J. Immunol*. 167:4271–4275.

Faleo, G., C. Fotino, N. Bocca, R.D. Molano, E. Zahr-Akrawi, J. Molina, S. Villate, O. Umland, J.S. Skyler, A.L. Bayer, et al. 2012. Prevention of autoimmune diabetes and induction of β-cell proliferation in NOD mice by hyperbaric oxygen therapy. *Diabetes*. 61:1769–1778. http://dx.doi.org/10.2337/db11-0516

Feuerer, M., Y. Shen, D.R. Littman, C. Benoist, and D. Mathis. 2009. How punctual ablation of regulatory T cells unleashes an autoimmune lesion within the pancreatic islets. *Immunity*. 31:654–664. http://dx.doi.org/10.1016/j.immuni.2009.08.023

Fife, B.T., K.E. Pauken, T.N. Eagar, T. Obu, J. Wu, Q. Tang, M. Azuma, M.F. Krummel, and J.A. Bluestone. 2009. Interactions between PD-1 and PD-L1 promote tolerance by blocking the TCR-induced stop signal. *Nat. Immunol*. 10:1185–1192. http://dx.doi.org/10.1038/ni.1790

Germain, R.N., E.A. Robey, and M.D. Cahalan. 2012. A decade of imaging cellular motility and interaction dynamics in the immune system. *Science*. 336:1676–1681. http://dx.doi.org/10.1126/science.1221063

Hadjantonakis, A.K., S. Macmaster, and A. Nagy. 2002. Embryonic stem cells and mice expressing different GFP variants for multiple non-invasive reporter usage within a single animal. *BMC Biotechnol*. 2:11. http://dx.doi.org/10.1186/1472-6750-2-11

Hagness, M., K. Henjum, J. Landskron, K.W. Brudvik, B.A. Bjørnbeth, A. Foss, K. Taskén, and E.M. Aandahl. 2012. Kinetics and activation requirements of contact-dependent immune suppression by human regulatory T cells. *J. Immunol*. 188:5459–5466. http://dx.doi.org/10.4049/jimmunol.1101367

Hahn, S., R. Gehri, and P. Erb. 1995. Mechanism and biological significance of CD4-mediated cytotoxicity. *Immunol. Rev.* 146:57–79. http://dx.doi.org/10.1111/j.1600-065X.1995.tb00684.x

Han, D., X. Cai, J. Wen, N.S. Kenyon, and Z. Chen. 2012. From biomarkers to a clue of biology: a computation-aided perspective of immune gene expression profiles in human type 1 diabetes. *Front Immunol*. 3:320.

Hara, M., R.F. Dizon, B.S. Glick, C.S. Lee, K.H. Kaestner, D.W. Piston, and V.P. Bindokas. 2006. Imaging pancreatic beta-cells in the intact pancreas. *Am. J. Physiol. Endocrinol. Metab.* 290:E1041–E1047. http://dx.doi.org/10.1152/ajpendo.00365.2005

Hogquist, K.A., S.C. Jameson, W.R. Heath, J.L. Howard, M.J. Bevan, and F.R. Carbone. 1994. T cell receptor antagonist peptides induce positive selection. *Cell*. 76:17–27. http://dx.doi.org/10.1016/0092-8674(94)90169-4

Huang, Y.H., D.K. Sojka, and D.J. Fowell. 2012. Cutting edge: Regulatory T cells selectively attenuate, not terminate, T cell signaling by disrupting NF-κB nuclear accumulation in CD4 T cells. *J. Immunol*. 188:947–951. http://dx.doi.org/10.4049/jimmunol.1101027

Josefowicz, S.Z., L.F. Lu, and A.Y. Rudensky. 2012. Regulatory T cells: mechanisms of differentiation and function. *Annu. Rev. Immunol*. 30:531–564. http://dx.doi.org/10.1146/annurev.immunol.25.022106.141623

Katz, J.D., B. Wang, K. Haskins, C. Benoist, and D. Mathis. 1993. Following a diabetogenic T cell from genesis through pathogenesis. *Cell*. 74:1089–1100. http://dx.doi.org/10.1016/0092-8674(93)90730-E

Kurts, C., W.R. Heath, F.R. Carbone, J. Allison, J.F. Miller, and H. Kosaka. 1996. Constitutive class I-restricted exogenous presentation of self antigens in vivo. *J. Exp. Med*. 184:923–930. http://dx.doi.org/10.1084/jem.184.3.923

Lu, Y., J. Suzuki, M. Guillioli, O. Umland, and Z. Chen. 2011. Induction of self-antigen-specific Foxp3+ regulatory T cells in the periphery by lymphodepletion treatment with anti-mouse thymocyte globulin in mice. *Immunology*. 134:50–59. http://dx.doi.org/10.1111/j.1365-2567.2011.03466.x

Lu, Y., H. Schneider, and C.E. Rudd. 2012. Murine regulatory T cells differ from conventional T cells in resisting the CTLA-4 reversal of TCR stop-signal. *Blood*. 120:4560–4570. http://dx.doi.org/10.1182/blood-2012-04-421420

Mandl, J.N., R. Liou, F. Klauschen, N. Vrisekoop, J.P. Monteiro, A.J. Yates, A.Y. Huang, and R.N. Germain. 2012. Quantification of lymph node transit times reveals differences in antigen surveillance strategies of naive CD4+ and CD8+ T cells. *Proc. Natl. Acad. Sci. USA*. 109:18036–18041. http://dx.doi.org/10.1073/pnas.1211717109

Mathis, D., and C. Benoist. 2004. Back to central tolerance. *Immunity*. 20:509–516. http://dx.doi.org/10.1016/S1074-7613(04)00111-6

Mempel, T.R., M.J. Pittet, K. Khazaie, W. Weninger, R. Weissleder, H. von Boehmer, and U.H. von Andrian. 2006. Regulatory T cells reversibly suppress cytotoxic T cell function independent of effector differentiation. *Immunity*. 25:129–141. http://dx.doi.org/10.1016/j.immuni.2006.04.015

Miska, J., E. Bas, P. Devarajan, and Z. Chen. 2012. Autoimmunity-mediated antitumor immunity: tumor as an immunoprivileged self. *Eur. J. Immunol*. 42:2584–2596. http://dx.doi.org/10.1002/eji.201242590

Mukhopadhaya, A., T. Hanafusa, I. Jarchum, Y.G. Chen, Y. Iwai, D.V. Serreze, R.M. Steinman, K.V. Tarbell, and T.P. DiLorenzo. 2008. Selective delivery of beta cell antigen to dendritic cells in vivo leads to deletion and tolerance of autoreactive CD8+ T cells in NOD mice. *Proc. Natl. Acad. Sci. USA*. 105:6374–6379. http://dx.doi.org/10.1073/pnas.0802644105

Nakamura, K., A. Kitani, and W. Strober. 2001. Cell contact-dependent immunosuppression by CD4(+)CD25(+) regulatory T cells is mediated by cell surface-bound transforming growth factor beta. *J. Exp. Med*. 194:629–644. http://dx.doi.org/10.1084/jem.194.5.629

Onishi, Y., Z. Fehervari, T. Yamaguchi, and S. Sakaguchi. 2008. Foxp3+ natural regulatory T cells preferentially form aggregates on dendritic cells in vitro and actively inhibit their maturation. *Proc. Natl. Acad. Sci. USA*. 105:10113–10118. http://dx.doi.org/10.1073/pnas.0711106105

Paust, S., L. Lu, N. McCarty, and H. Cantor. 2004. Engagement of B7 on effector T cells by regulatory T cells prevents autoimmune disease. *Proc. Natl. Acad. Sci. USA*. 101:10398–10403. http://dx.doi.org/10.1073/pnas.0403342101

Piccirillo, C.A., and E.M. Shevach. 2001. Cutting edge: control of CD8+ T cell activation by CD4+CD25+ immunoregulatory cells. *J. Immunol*. 167:1137–1140.

Pierson, W., B. Cauwe, A. Policheni, S.M. Schlenner, D. Franckaert, J. Berges, S. Humblet-Baron, S. Schönefeldt, M.J. Herold, D. Hildeman, et al. 2013. Antiapoptotic Mcl-1 is critical for the survival and niche-filling capacity of Foxp3$^+$ regulatory T cells. *Nat. Immunol*. 14:959–965. http://dx.doi.org/10.1038/ni.2649

Read, S., V. Malmström, and F. Powrie. 2000. Cytotoxic T lymphocyte-associated antigen 4 plays an essential role in the function of CD25(+)CD4(+) regulatory cells that control intestinal inflammation. *J. Exp. Med*. 192:295–302. http://dx.doi.org/10.1084/jem.192.2.295

Ricordi, C., P.E. Lacy, K. Sterbenz, and J.M. Davie. 1987. Low-temperature culture of human islets or in vivo treatment with L3T4 antibody produces a marked prolongation of islet human-to-mouse xenograft survival. *Proc. Natl. Acad. Sci. USA*. 84:8080–8084. http://dx.doi.org/10.1073/pnas.84.22.8080

Rodriguez-Diaz, R., M.H. Abdulreda, A.L. Formoso, I. Gans, C. Ricordi, P.O. Berggren, and A. Caicedo. 2011. Innervation patterns of autonomic axons in the human endocrine pancreas. *Cell Metab.* 14:45–54. http://dx.doi.org/10.1016/j.cmet.2011.05.008

Ruocco, M.G., K.A. Pilones, N. Kawashima, M. Cammer, J. Huang, J.S. Babb, M. Liu, S.C. Formenti, M.L. Dustin, and S. Demaria. 2012. Suppressing T cell motility induced by anti-CTLA-4 monotherapy improves antitumor effects. *J. Clin. Invest.* 122:3718–3730. http://dx.doi.org/10.1172/JCI61931

Samy, E.T., L.A. Parker, C.P. Sharp, and K.S. Tung. 2005. Continuous control of autoimmune disease by antigen-dependent polyclonal CD4+CD25+ regulatory T cells in the regional lymph node. *J. Exp. Med.* 202:771–781. http://dx.doi.org/10.1084/jem.20041033

Schneider, H., J. Downey, A. Smith, B.H. Zinselmeyer, C. Rush, J.M. Brewer, B. Wei, N. Hogg, P. Garside, and C.E. Rudd. 2006. Reversal of the TCR stop signal by CTLA-4. *Science.* 313:1972–1975. http://dx.doi.org/10.1126/science.1131078

Sherry, N.A., J.A. Kushner, M. Glandt, T. Kitamura, A.M. Brillantes, and K.C. Herold. 2006. Effects of autoimmunity and immune therapy on beta-cell turnover in type 1 diabetes. *Diabetes.* 55:3238–3245. http://dx.doi.org/10.2337/db05-1034

Shevach, E.M. 2006. From vanilla to 28 flavors: multiple varieties of T regulatory cells. *Immunity.* 25:195–201. http://dx.doi.org/10.1016/j.immuni.2006.08.003

Shevach, E.M. 2008. Immunology. Regulating suppression. *Science.* 322:202–203. http://dx.doi.org/10.1126/science.1164872

Shevach, E.M. 2011. Biological functions of regulatory T cells. *Adv. Immunol.* 112:137–176. http://dx.doi.org/10.1016/B978-0-12-387827-4.00004-8

Speier, S., D. Nyqvist, O. Cabrera, J. Yu, R.D. Molano, A. Pileggi, T. Moede, M. Köhler, J. Wilbertz, B. Leibiger, et al. 2008a. Noninvasive in vivo imaging of pancreatic islet cell biology. *Nat. Med.* 14:574–578. http://dx.doi.org/10.1038/nm1701

Speier, S., D. Nyqvist, M. Köhler, A. Caicedo, I.B. Leibiger, and P.O. Berggren. 2008b. Noninvasive high-resolution in vivo imaging of cell biology in the anterior chamber of the mouse eye. *Nat. Protoc.* 3:1278–1286. http://dx.doi.org/10.1038/nprot.2008.118

Stadinski, B.D., T. Delong, N. Reisdorph, R. Reisdorph, R.L. Powell, M. Armstrong, J.D. Piganelli, G. Barbour, B. Bradley, F. Crawford, et al. 2010. Chromogranin A is an autoantigen in type 1 diabetes. *Nat. Immunol.* 11:225–231. http://dx.doi.org/10.1038/ni.1844

Surh, C.D., and J. Sprent. 2008. Homeostasis of naive and memory T cells. *Immunity.* 29:848–862. http://dx.doi.org/10.1016/j.immuni.2008.11.002

Tadokoro, C.E., G. Shakhar, S. Shen, Y. Ding, A.C. Lino, A. Maraver, J.J. Lafaille, and M.L. Dustin. 2006. Regulatory T cells inhibit stable contacts between CD4+ T cells and dendritic cells in vivo. *J. Exp. Med.* 203:505–511. http://dx.doi.org/10.1084/jem.20050783

Takahashi, T., Y. Kuniyasu, M. Toda, N. Sakaguchi, M. Itoh, M. Iwata, J. Shimizu, and S. Sakaguchi. 1998. Immunologic self-tolerance maintained by CD25+CD4+ naturally anergic and suppressive T cells: induction of autoimmune disease by breaking their anergic/suppressive state. *Int. Immunol.* 10:1969–1980. http://dx.doi.org/10.1093/intimm/10.12.1969

Tang, Q., J.Y. Adams, A.J. Tooley, M. Bi, B.T. Fife, P. Serra, P. Santamaria, R.M. Locksley, M.F. Krummel, and J.A. Bluestone. 2006. Visualizing regulatory T cell control of autoimmune responses in nonobese diabetic mice. *Nat. Immunol.* 7:83–92. http://dx.doi.org/10.1038/ni1289

Tarbell, K.V., L. Petit, X. Zuo, P. Toy, X. Luo, A. Mqadmi, H. Yang, M. Suthanthiran, S. Mojsov, and R.M. Steinman. 2007. Dendritic cell-expanded, islet-specific CD4+ CD25+ CD62L+ regulatory T cells restore normoglycemia in diabetic NOD mice. *J. Exp. Med.* 204:191–201. http://dx.doi.org/10.1084/jem.20061631

Teft, W.A., M.G. Kirchhof, and J. Madrenas. 2006. A molecular perspective of CTLA-4 function. *Annu. Rev. Immunol.* 24:65–97. http://dx.doi.org/10.1146/annurev.immunol.24.021605.090535

Thornton, A.M., and E.M. Shevach. 1998. CD4+CD25+ immunoregulatory T cells suppress polyclonal T cell activation in vitro by inhibiting interleukin 2 production. *J. Exp. Med.* 188:287–296. http://dx.doi.org/10.1084/jem.188.2.287

Tisch, R., and B. Wang. 2008. Dysrulation of T cell peripheral tolerance in type 1 diabetes. *Adv. Immunol.* 100:125–149. http://dx.doi.org/10.1016/S0065-2776(08)00805-5

Tite, J.P., and C.A. Janeway Jr. 1984. Cloned helper T cells can kill B lymphoma cells in the presence of specific antigen: Ia restriction and cognate vs. noncognate interactions in cytolysis. *Eur. J. Immunol.* 14:878–886. http://dx.doi.org/10.1002/eji.1830141004

Tsai, S., P. Serra, X. Clemente-Casares, R.M. Slattery, and P. Santamaria. 2013. Dendritic cell-dependent in vivo generation of autoregulatory T cells by antidiabetogenic MHC class II. *J. Immunol.* 191:70–82. http://dx.doi.org/10.4049/jimmunol.1300168

Turley, S., L. Poirot, M. Hattori, C. Benoist, and D. Mathis. 2003. Physiological beta cell death triggers priming of self-reactive T cells by dendritic cells in a type-1 diabetes model. *J. Exp. Med.* 198:1527–1537. http://dx.doi.org/10.1084/jem.20030966

Wan, Y.Y., and R.A. Flavell. 2005. Identifying Foxp3-expressing suppressor T cells with a bicistronic reporter. *Proc. Natl. Acad. Sci. USA.* 102:5126–5131. http://dx.doi.org/10.1073/pnas.0501701102

Wing, K., Y. Onishi, P. Prieto-Martin, T. Yamaguchi, M. Miyara, Z. Fehervari, T. Nomura, and S. Sakaguchi. 2008. CTLA-4 control over Foxp3+ regulatory T cell function. *Science.* 322:271–275. http://dx.doi.org/10.1126/science.1160062

Yi, P., J.S. Park, and D.A. Melton. 2013. Betatrophin: a hormone that controls pancreatic β cell proliferation. *Cell.* 153:747–758. http://dx.doi.org/10.1016/j.cell.2013.04.008

Zhang, N., B. Schröppel, G. Lal, C. Jakubzick, X. Mao, D. Chen, N. Yin, R. Jessberger, J.C. Ochando, Y. Ding, and J.S. Bromberg. 2009. Regulatory T cells sequentially migrate from inflamed tissues to draining lymph nodes to suppress the alloimmune response. *Immunity.* 30:458–469. http://dx.doi.org/10.1016/j.immuni.2008.12.022